UNIVERSITY OF LEEDS

This is a repository copy of *Enhanced stability and controlled gastrointestinal digestion of β-carotene loaded Pickering emulsions with particle–particle complex interfaces*.

White Rose Research Online URL for this paper:
https://eprints.whiterose.ac.uk/179411/

Version: Accepted Version

Article:
Wei, Y, Zhang, L, Liao, W et al. (7 more authors) (2021) Enhanced stability and controlled gastrointestinal digestion of β-carotene loaded Pickering emulsions with particle–particle complex interfaces. Food & Function, 2021 (21). pp. 10842-10861. ISSN 2042-6496

https://doi.org/10.1039/d1fo01714d

© The Royal Society of Chemistry 2021. This is an author produced version of an article published in Food & Function. Uploaded in accordance with the publisher's self-archiving policy.

Reuse
Items deposited in White Rose Research Online are protected by copyright, with all rights reserved unless indicated otherwise. They may be downloaded and/or printed for private study, or other acts as permitted by national copyright laws. The publisher or other rights holders may allow further reproduction and re-use of the full text version. This is indicated by the licence information on the White Rose Research Online record for the item.

Takedown
If you consider content in White Rose Research Online to be in breach of UK law, please notify us by emailing eprints@whiterose.ac.uk including the URL of the record and the reason for the withdrawal request.

White Rose university consortium
Universities of Leeds, Sheffield & York

eprints@whiterose.ac.uk
https://eprints.whiterose.ac.uk/

This document is confidential and is proprietary to the American Chemical Society and its authors. Do not copy or disclose without written permission. If you have received this item in error, notify the sender and delete all copies.

Zein Colloidal Particles and Cellulose Nanocrystals Synergistic Stabilization of Pickering Emulsions for Delivery of β-Carotene

Journal:	*Journal of Agricultural and Food Chemistry*
Manuscript ID	jf-2020-07800h.R3
Manuscript Type:	Article
Date Submitted by the Author:	n/a
Complete List of Authors:	Wei, Yang; China Agricultural University, Food Science and Nutritional Engineering; University of Leeds, School of Food Science and Nutrition Liu, Zikun; China Agricultural University, Food Science and Nutritional Engineering Guo, Aixin; China Agricultural University, Food Science and Nutritional Engineering Mackie, Alan; University of Leeds, School of Food Science and Nutrition Zhang, Liang; China Agricultural University, Food Science and Nutritional Engineering Liao, Wenyan; China Agricultural University, Food Science and Nutritional Engineering Mao, Like; China Agricultural University - East Campus, College of Food Science and Nutritional Engineering Yuan, Fang; China Agricultural University, College of Food Science & Nutritional Engineering Gao, Yanxiang; China Agricultural University, Food Science and Nutritional Engineering

SCHOLARONE™
Manuscripts

Zein Colloidal Particles and Cellulose Nanocrystals Synergistic Stabilization of Pickering Emulsions for Delivery of β-Carotene

*Yang Wei [a, b], Zikun Liu [a], Aixin Guo [a], Alan Mackie [b], Liang Zhang [a], Wenyan Liao [a], Like Mao [a], Fang Yuan [a], Yanxiang Gao [a]**

[a]*Beijing Key Laboratory of Functional Food from Plant Resources, College of Food Science & Nutritional Engineering, China Agricultural University, Beijing, 100083, P. R. China*

[b]*Food Colloids and Processing Group, School of Food Science and Nutrition, University of Leeds, Leeds LS2 9JT, UK*

*Corresponding author.

Tel.: + 86-10-62737034 Fax: + 86-10-62737986 Address: Box 112, No.17 Qinghua East Road, Haidian District, Beijing 100083, China

E-mail: gyxcau@126.com

Abstract:

In this study, we utilized different types of particles to stabilize β-carotene loaded Pickering emulsions: spherical hydrophobic zein colloidal particles (ZCPs) (517.3 nm) and rod-shaped hydrophilic cellulose nanocrystals (CNCs) (115.2 nm). Either of the particles was incapable of stabilizing Pickering emulsions owing to their inappropriate wettability. When the mass ratio of ZCPs and CNCs was 1:4, the Pickering emulsion showed the best physical and photothermal stability. Compared to the ZCP-stabilized Pickering emulsion (9.29%), the retention rate of β-carotene in the Pickering emulsion co-stabilized by ZCPs and CNCs was elevated to 60.23% after 28 days of storage at 55 ℃. Confocal microscopy and cryo-scanning electron microscopy confirmed that different types of particles could form a multilayerd structure or induce the formation of the interparticle network. Furthermore, the complexation of ZCPs and CNCs delayed the lipolysis of the emulsion during *in vitro* digestion. The free fatty acid (FFA) release rate of Pickering emulsions in the small intestinal phase was reduced from 19.46% to 8.73%. Accordingly, the bioaccessibility of β-carotene in Pickering emulsions ranged from 9.14% to 27.25% through adjusting the mass ratio and addition sequence of distinct particles at the interface. The Pickering emulsion with the novel particle-particle complex interface was designed in foods and pharmaceuticals for purpose of enhanced stability, delayed lipolysis or sustained nutrient release.

Keywords: Pickering emulsion; β-Carotene; Zein colloidal particle; Cellulose nanocrystals; Particle-particle complex interface; *In vitro* digestion

1. Introduction

The emulsions with adsorbed colloidal particles to stabilize the liquid-liquid interface are defined as Pickering emulsions.[1] Particles with an intermediate wettability can facilitate the attachment of particles to the interface instead of the predominant distribution in the water or oil phase and increase the energy required for their desorption from the interface. Therefore, the particles attached at the interface confer the Pickering emulsion a great ability to resist coalescence or Ostwald ripening.[2] Compared with the traditional emulsions stabilized by surfactants or polymers, Pickering emulsions show a superior stability against coalescence, high internal phase proportion, stimuli responsiveness and modulation of lipid digestion. Recently, a significant portion of the research has focused on the design of suitable particles to stabilize food grade Pickering emulsions. The ingredients for making Pickering particles can be synthetic or natural polymeric materials, including surfactants, phospholipids, proteins, polyphenols, and polysaccharides.[3,4] However, the intricate production of the complex particles restricts their large-scale commercial application.

Within a real food matrix, particles, biosurfactants and biopolymers often occur at the interface simultaneously, e.g., particles-biopolymers, particles-biosurfactants, and biopolymers-biosurfactants.[5–8] Because of the diversity in molecular structure, surface charge, addition sequence and mass ratio between different surface-active components, the emulsions can form various microstructures depending on their interfacial composition.[9,10] Nevertheless, the interaction between different particles in

the bulk phase or at the interface and their impact on the stability and digestion behavior of Pickering emulsions have received limited attention. Sarkar et al. (2018) reported the production of Pickering emulsions using a composite layer of lactoferrin nanogel particles and inulin nanoparticles as a steric barrier to delay gastric digestion.[11] Various nanoparticles possess distinct hydrophilic/hydrophobic properties, morphologies, sizes and surface charges. These characteristics affect the inter-particle interaction and their adsorption and alignment at the interface, further impacting the interaction between the droplets.[12,13] Due to these unique properties, the complex interface composed of different particles can exhibit diverse structures that exert a vital role in stabilizing emulsions and delivering multiple nutraceuticals or drugs, and have a promising potential in developing fat substitutes and porous materials through strengthening steric barriers to the interfacial disproportionation and coalescence.[13]

Cellulose nanocrystals (CNCs) are rod-shaped nanoparticles with high crystallinity, usually extracted from different bioresources.[14] CNCs are traditionally produced by sulfuric acid hydrolysis generated with anionic sulfate half-ester groups, which can prepare stable aqueous suspensions except under strong acid and high ionic strength.[15] The superiority of CNCs in food and pharmaceutical industries stems from their advantages such as high surface-area-to-volume ratio and excellent physicochemical stability.[16,17] The high aspect ratio provides CNCs with better mechanical properties and thermal stability, as well as unique rheological and optical properties, and also promotes the interconnection between CNCs during film

formation and interfacial adsorption. Owing to these advantages and environmental sustainability, CNCs show the promising applications in commercial formulations such as biomedicines, packaging and personal care supplies.[18] Despite CNCs are recognized as hydrophilic (due to extensive hydroxylation), the highly ordered polymer chains endow the nanocrystals with amphiphilic properties due to a ''hydrophobic edge''.[19–21] Unmodified CNCs can stabilize emulsions with a low surface charge density,[22] because CNCs at the interface form a diluted mesh network within the interconnected droplets.[14,23] The combination of CNCs and other components for creating a stable emulsion has also been explored, such as polysaccharides, proteins, surfactants, and particles.[14,18] Unlike chemical modification of CNCs, these complex interfaces involving CNCs are generally formed by noncovalent interactions, thus adjusting surface hydrophobicity and interfacial structure in a more economically and environmentally friendly way.[24] As a dietary fiber that is undigestible in the upper digestive tract, CNCs can effectively inhibit lipid hydrolysis and ingestion when adsorbed on the surface of the lipid droplets, which is beneficial to prevent obesity and a variety of chronic diseases.

Zein, the major storage protein of maize, can be fabricated into colloidal particles (ZCPs) through self-assembly.[25] Although ZCP is regarded as a common Pickering stabilizer, the ZCP-stabilized Pickering emulsion is unstable due to the hydrophobicity of interfacial particles.[26] Many strategies have been proposed to control the interfacial wettability of zein-based particles through complexing with other ingredients, such as proteins, polysaccharides, and surfactants, which require a

precise design and safety assessment.[27,28] In addition, the Pickering emulsion stabilized by ZCPs alone has a large inter-particle space on the surface of the droplet, which results in the digestive components in the gastrointestinal tract that can be adsorbed to the droplet surface and cause lipid hydrolysis. Neither the hydrophobic ZCPs nor the hydrophilic CNCs have a suitable wettability to stabilize Pickering emulsions alone. Due to the requirements of environmental sustainability and cumbersome production process, this study did not directly utilize chemical modification or prepare complex particles, but the combination of ZCPs and CNCs was applied to prepare Pickering emulsions with particle-particle complex interfaces. The incorporation of CNCs could improve the hydrophobicity of interfacial particles and reduce the accessible surface area of emulsion droplets, which might enhance the stability of Pickering emulsions and restrict the lipid digestion.

The objective of this study was to fabricate the Pickering emulsion co-stabilized by ZCPs and CNCs, and to investigate the effects of the mass ratio and sequence of mixed particles on the properties of Pickering emulsions with the complex particle-particle interface. We aimed to utilize distinct but imperfect particles with different characteristics to synergistically stabilize the oil-water interface instead of constructing composite particles. Subsequently, the physicochemical stability of β-carotene loaded Pickering emulsions under different stresses were tested. *In vitro* gastrointestinal digestion of Pickering emulsions was determined, and the influence of interfacial composition on the lipolysis and bioaccessibility of β-carotene was investigated.

2. Materials and methods

2.1. Materials

Zein (protein content: 91.3%), porcine pancreatic lipase type 2 (L3126) and bile salts (1:1 mixture of cholic acid and deoxycholic acid, 48305) were purchased from Sigma-Aldrich (USA). The CNCs with a diameter of 5–20 nm and length of 100–200 nm was obtained from Shanghai ScienceK Nanotechnology Ltd. Cellulose nanocrystals (CNCs) were isolated by sulfuric acid hydrolysis of wood fibers. Medium-chain triglycerides (MCT, Miglyol 812N) were purchased from Musim Mas (Medan, Indonesia). β-Carotene suspension (30% by mass β-carotene in sunflower oil) was supplied by Xinchang Pharmaceutical Company, Ltd. (Xinchang, Zhejiang, China). Absolute ethanol (99.99%), solid sodium hydroxide and liquid hydrochloric acid (36%, w/w) were obtained from Eshowbokoo Biological Technology Co., Ltd. (Beijing, China). All other chemical agents were of analytical grade.

2.2. Preparation of ZCPs and CNCs

Zein colloidal particles (ZCPs) were fabricated through the solvent-evaporation method.[29] Briefly, 3.0 g zein was dissolved in 300 mL 70% (v/v) aqueous ethanol solution and stirred at 600 rpm overnight at 25 ℃. The ethanol in the solution was then removed at 45 ℃ for 25 min through rotary evaporation and the remaining

131 volume was set to be around 100 mL. The sample was diluted with pH-adjusted water
132 (pH 4.0) to 150 mL. The ZCPs suspension was centrifuged at 3000 rpm for 10 min to
133 separate any large aggregates if any. Finally, the supernatant obtained was adjusted to
134 pH 4.0 by using 0.1 M HCl solution.

135 The CNC suspension with the desired concentration was obtained by dispersing
136 1.5 g CNC powder into 100 mL deionized water and followed by ultrasonic treatment
137 (10 min, 400 W) using probe-type sonicator. The pH of the CNC suspension was
138 adjusted to 4.0 by adding 0.1 M HCl or NaOH. In all samples, 50 mM NaCl was
139 maintained in the aqueous phase to partially screen the surface charge of CNCs and
140 promote their interfacial packing.

141

142 *2.3. Characterization of ZCPs and CNCs*

143 The particle size (Z-average size) and zeta-potential of ZCPs and CNCs were
144 determined by a Zetasizer (Nano-ZS90, Malvern Instruments Ltd., Worcestershire,
145 UK). The type of cuvette used was DTS1060 and the scattering angle was 90°.
146 Samples were diluted with distilled water to avoid multiple light scattering effects.
147 Thereafter, the samples were adjusted to pH 4.0 to measure the particle size and
148 zeta-potential.[29] All measurements were conducted in triplicate.

149 The morphology of ZCPs and CNCs was captured with Tecnai 200 transmission
150 electron microscope (FEI Company, Eindhoven, Netherlands) under 60 kV
151 accelerating voltage. The particle concentration was diluted to 0.2 mg/mL and one
152 drop of the dispersions was placed on a 200-mesh carbon-coated copper grid. Images

153 with various magnifications were taken at 25 kV.

154 The morphological features of CNCs were observed with AFM (Veeco
155 Company, Plainview, NY, USA) equipped with an E-scanner. Tapping mode was
156 used with a nominal spring constant of 20–100 Nm^{-1} and nominal resonance
157 frequencies of 10–200 kHz. Briefly, 10 μL sample was dropped onto freshly cleaved
158 mica sheets mounted on sample disks and air dried for more than 2 h before scanning.

159 The contact angles of ZCPs and CNCs were measured with an OCA 20 AMP
160 (Dataphysics Instruments GmbH, Filderstadt, Germany). All the measurements were
161 conducted in triplicate and averaged. The freeze-dried samples were compressed to
162 obtain tablets with 2 mm thickness and 13 mm diameter. Then the tablets were placed
163 into an optical glass cuvette, which contained MCT. Next, about 2 μL of deionized
164 water was deposited on the surface of the tablets using a high precision injector. After
165 the equilibrium was attained, images of the drops formed were acquired using a
166 digital camera and the $\theta_{o/w}$ value was calculated based on the LaPlace−Young
167 equation.[27] Measurements were averaged over at least three drops.

168

169 *2.4. Fabrication of β-carotene loaded Pickering emulsions*

170 β-Carotene suspension (20 g) was first dissolved in MCT (180 g) to form oil
171 phase (3.0 wt% β-carotene).

172 **Method I:** The primary emulsion was fabricated by mixing different quantities
173 of ZCPs (3.0%, w/w) suspension with 15 g of oil phase at 18000 rpm by a blender
174 (Ultra Turrax, model T25, IKA Labortechnic, Staufen, Germany). After the complete

dispersion of oil phase, the mixture was further homogenized for another 5 min. Secondary emulsions were fabricated by mixing the primary emulsion with different amounts of CNCs suspension (1.5%, w/w) and homogenized under the same condition. The total weight of ZCPs and CNCs suspensions was set to be 15 g, and the mass ratios of ZCPs to CNCs were designed to be 4:1, 2:1, 1:1, 1:2, and 1:4, respectively. The Pickering emulsions were termed as 4Z1C, 2Z1C, 1Z1C, 1Z2C, and 1Z4C according to the mass ratios of ZCPs to CNCs. The pH of fresh emulsions was adjusted to 4.0.

Method II: The primary emulsion was fabricated by mixing different quantities of CNCs (1.5%, w/w) suspension with 15 g of oil phase at 18000 rpm using a blender (Ultra Turrax, model T25, IKA Labortechnic, Staufen, Germany). After the complete dispersion of oil phase, the mixture was further homogenized for another 5 min. Secondary emulsions were fabricated by mixing the primary emulsion with different quantities of ZCPs suspension (3.0%, w/w) and homogenized under the same condition. The total weight of ZCPs and CNCs suspensions was set to be 15 g, and the mass ratios of CNCs to ZCPs were designed to be 4:1, 2:1, 1:1, 1:2, and 1:4, respectively. The Pickering emulsions were termed as 4C1Z, 2C1Z, 1C1Z, 1C2Z, and 1C4Z based on the mass ratios of CNCs to ZCPs. The pH of different Pickering emulsions was adjusted to 4.0 using 0.5 M HCl.

Control groups: The Pickering emulsion was prepared by homogenizing 15.0 g of ZCPs (3.0%, w/w) or CNCs (1.5%, w/w) suspension with 15.0 g of oil phase through the same procedure and termed as ZCPs and CNCs.

197

198 *2.5. Droplet size and zeta-potential*

199 The droplet size was determined after emulsion preparation for 12 h with a laser
200 scattering size analyzer (LS230®, Beckman Coulter, Brea, CA, USA). The emulsions
201 were diluted with deionized water and stirred to reach an obscuration rate between 8%
202 to 12%. The optical parameters were applied as follows: a refractive indice of 1.52 for
203 MCT and absorption of 0.001, and a refractive indice of 1.33 for the dispersant
204 (deionized water).[8] The volume-area ($D_{4,3}$) average diameter was calculated by using
205 the following equation 1:

206 $$D4,3 = \frac{\sum nidi^4}{\sum nidi^3} \quad (1)$$

207 The n_i is the number of particles with a diameter of d_i.

208 The zeta-potential was measured according to the direction and velocity of
209 droplet movement in a well-defined electric field using a Zetasizer NanoZS90
210 (Malvern Instruments, Worcestershire, UK). The droplet concentration of emulsions
211 were diluted to 0.005 wt% to minimize multiple scattering effects. The data were
212 collected from at least 10 sequential readings per sample after 120 s of equilibration
213 and calculated by the instrument based on the Smoluchowski model.

214

215 *2.6. Rheological properties*

216 The rheological properties were measured at 25 °C with an AR-1500 rheometer
217 (TA Instruments, West Sussex, UK) using a steel parallel plate (40 mm diameter, gap
218 0.100 mm). The samples were deposited onto the plate and allowed to reach

219 temperature equilibrium for 5 min. For the steady-state flow measurement, the shear
220 rate ranged from 0.1 to 100 s^{-1}, and the apparent viscosity (η) was collected. All the
221 dynamic tests were performed within the linear viscoelastic region, and a stress value
222 of 1 Pa was chosen for the frequency test. Frequency was oscillated between 0.1 to
223 100 rad/s and strain was performed at 1%.[8] Both storage modulus (G ′) and loss
224 modulus (G ″) were recorded as a function of frequency to determine whether the
225 emulsion was strongly or weakly flocculated.
226
227 *2.7. Physicochemical stability of β-carotene loaded Pickering emulsions*
228 *2.7.1. Physical stability*
229 The physical stability of Pickering emulsions was analyzed with the LUMiSizer
230 (L.U.M. 290 GmbH, Germany) based on the principle that the centrifugation
231 accelerates the destabilization. Specifically, 1.8 mL of sample was centrifugated at
232 3000 rpm for 1 h at 25 °C with the fixed interval of 20 s.
233 *2.7.2. Effect of UV radiation*
234 The photostability of β-carotene under ultraviolet (UV) radiation was evaluated.[8]
235 Briefly, the transparent glass vials containing 15 g of samples were transferred into
236 transparent glass bottles in a controlled light cabinet (0.68 W/m^2, 45 ℃, QSUN
237 Xe-1-B, Q-Lab Corporation, Ohio, USA) for 4 h. The content of β-carotene was
238 plotted against treatment time. The β-carotene in the emulsions was extracted three
239 times with a mixture of 1 mL ethanol and 3 mL of n-hexane. After adding the organic

reagents, the mixed solution was vortexed for 2 min, and the supernatant was obtained after centrifugation at 3000 rpm for 10 min. Collect the supernatant obtained after three extractions and dilute to 10 mL. The β-carotene in the supernatant was further diluted to an appropriate concentration by n-hexane. And then the absorbance at 450 nm was measured with a UV-1800 UV–vis spectrophotometer (Shimadzu, Kyoto, Japan).[30]

2.7.3. Effect of thermal treatment

The samples after 12 h storage at 25 ℃ were incubated at 90 ℃ for 60 min and then cooled down to 25 ℃.[8] The droplet size, zeta-potential, and retention rate of β-carotene were determined after thermal treatment.

2.7.4. Effect of pH

The influence of pH on the stability of Pickering emulsions was tested following a previous report.[31] The prepared emulsions after 12 h storage at 25 ℃ were adjusted to pH 2.5, 6.0 and 8.5 by 0.1 M NaOH or 0.1 M HCl.

2.7.5. Effect of ionic strength

Different weight of NaCl powder was mixed with the prepared emulsions after 12 h storage at 25 ℃ for 2 h. The NaCl concentrations of Pickering emulsions were adjusted to 10, 50 and 100 mM.[31]

2.7.6. Effect of storage time

After the preparation of Pickering emulsions, the fresh samples were stored at 55 ℃ for 4 weeks. The droplet size and retention rate of β-carotene in Pickering

emulsions were measured at regular storage periods (1, 7, 14, 21 and 28 days).

2.8. Confocal laser scanning microscopy (CLSM)

CLSM (Zeiss780, Oberkochen, Germany) was utilized to observe the microstructure of droplets. The emulsions were stained with a mixed fluorescent dye solution consisting of Nile blue (0.1% dissolved in absolute ethanol) and Nile red (0.1% dissolved in absolute ethanol). Then the dyed emulsions were deposited on concave confocal microscope slides and gently covered with a cover slip. The Nile blue was used to dye the ZCPs (red phase) and the Nile red was applied to stain the oil phase (green phase). The CLSM was operated with two laser excitation sources: an argon/krypton laser at 488nm (Nile red) and a Helium Neon laser (He-Ne) at 633 nm (Nile blue).[32]

2.9. Cryo-scanning electronic microscopy (Cryo-SEM)

The sample is vitrified with liquid nitrogen and maintained at a very low temperature, which preserves the microstructure of Pickering emulsions in a frozen state and allow them to remain stable during the observation.[32,33] The samples were placed on an aluminum platelet, and then transferred to a cryo-preparation system (PP3010T, Quorum Inc., Laughton, East Sussex, UK). The samples were freeze-fractured in the cryo-preparation chamber, coated with platinum. Then the images were taken through SEM (Helios NanoLab G3 UC, FEI, Hillsboro, OR, USA). The analysis was conducted at a working distance between 3 and 5 mm with

283 TLD detection at 2 kV.

284

285 *2.10. In vitro gastrointestinal digestion analysis*

286 An *in vitro* gastrointestinal model was applied in this study with some
287 modifications.[34] All samples and solutions were maintained at 37 ℃ throughout the
288 gastrointestinal digestion process.

289 *Stomach phase*: 20 mL of the emulsion was mixed with 20 mL of simulated
290 gastric fluid (SGF) containing 0.0032 g/mL pepsin to mimic gastric digestion. The pH
291 was adjusted to 2.0 and the sample was then swirled at 150 rpm for 1 h.

292 *Small intestine phase*: 20 mL of gastric digesta was transferred into a 100 mL
293 glass beaker and then adjusted to pH 7.0. Thereafter, 20 mL of simulated intestinal
294 fluid (SIF) containing 5 mg/mL bile salt, 0.4 mg/mL pancreatin and 3.2 mg/mL lipase
295 was mixed with digesta in reaction vessel. The pH was adjusted to 7.0 and the
296 samples were held under continuous stirring at 150 rpm for 2 h to mimic the small
297 intestine digestion.

298 The degree of lipolysis was measured through the quantity of free fatty acids
299 (FFA) released. The quantity of 0.5 M NaOH required to neutralize the released FFA
300 through lipid digestion was determined by a pH-stat automatic titration unit
301 (Metrohm, Switzerland, 916 Ti-Touch). The quantity of FFA released was determined
302 as the percentage of FFA (%) released during the digestion time as described by the
303 equation 2:[35]

304 $$\%FFA = \frac{V_{NaOH} m_{NaOH} M_{lipid}}{2W_{lipid}} \times 100 \quad (2)$$

where V_{NaOH} and m_{NaOH} represent the volume (L) and concentration (M) of NaOH solution needed to neutralize the FFA, respectively and W_{lipid} and M_{lipid} represent the initial mass (g) and molecular mass ($g \cdot mol^{-1}$) of the triacylglycerol oil, respectively.

The bioaccessibility of β-carotene was determined after the intestinal digestion [8]. Part of digesta was processed by using a high-speed centrifuge at 15,000 rpm for 60 min at 4 ℃. The micelle phase containing the solubilized β-carotene was collected. The content of β-carotene extracted from the initial emulsion and micelle fraction was determined according to the method described in 2.6.1. The bioaccessibility (%) of β-carotene was calculated by following the equation 3:

$$Bioaccessibility\ (\%) = \frac{C_{micelle}}{C_{initial\ emulsion}} \times 100 \quad (3)$$

where, $C_{micelle}$ and $C_{initial\ emulsion}$ are the contents of β-carotene in the micelle fraction and the initial emulsion.

2.11. Statistical analysis

All the measurements were triplicate and the data obtained were average values of three determinations, which were subjected to statistical analysis of variance with SPSS 18.0 (SPSS Inc., Chicago, USA). Statistical differences were determined by one-way analysis of variance (ANOVA) with Duncan's post hoc test and least significant differences ($p < 0.05$) were accepted among the treatments.

3. Results and discussion

3.1. Characteristics of ZCPs and CNCs

The ZCPs showed a spherical shape and high polydispersity in the particle size (Fig. 1A). The slight aggregation between the particles was observed due to their inherent hydrophobicity. The Z-average size and zeta-potential of ZCPs were 517.3 ± 10.6 nm and 35.40 ± 1.06 mV. The large size of ZCPs restricted their rate of adsorption to the oil/water interface, but endowed the resulting emulsion with an excellent stability owing to a high desorption energy, which was clarified by a classical literature.[36] The mean size of CNCs measured by DLS was 115.2 ± 1.3 nm and zeta-potential of CNCs was - 41.24 ± 1.32 mV. Fig. 1B and C demonstrate the TEM and AFM images of CNCs, respectively. The TEM image suggested that CNCs were stiff, needle-like particles with a nearly perfect crystalline structure, forming a compact network-type architecture, which was ascribed to the high aspect ratio of CNCs. The size and structure of CNCs observed were correlated with the morphology obtained by AFM. Fig. 1D shows the complexation of ZCPs and CNCs in the bulk phase at the mass ratio of 2:1. The CNCs were intensively adsorbed on the surface of larger ZCPs, which was mainly attributed to the opposite charges carried by different types of particles, resulting in a strong attraction between ZCPs and CNCs. It is worth noting that CNCs formed a multi-layer adsorption structure on the surface of ZCPs, and the interconnected CNCs network extended into the aqueous phase to form bridges.

Interfacial wettability is an vital indicator to assess the ability of particles to anchor at interfaces and generally expressed by the contact angle ($\theta_{o/w}$).[36] The $\theta_{o/w}$ of

ZCPs was 130.1 ° (Fig. 1E), indicating its strong hydrophobicity, which may cause severe droplet aggregation.[37] The result was consistent with the wettability of ZCPs fabricated by the solvent-evaporation method according to a previous study.[27] The CNCs exhibited strong hydrophilicity with a $\theta_{o/w}$ of 29.1 ° due to the high number of hydroxyl groups (Fig. 1F). This result indicated that CNCs were preferentially wetted by water rather than oil, which was consistent with the report of Hu et al. (2015).[14]

3.2. Droplet size and zeta-potential

As depicted in Fig. 2A, the Pickering emulsion solely stabilized by ZCPs showed the largest droplet size ($D_{4,3}$) (5.11 ± 0.04 μm). The hydrophobic attraction between ZCPs at interfaces was stronger than steric and electrostatic repulsion, which induced the aggregation between droplets. The droplet size of the CNC-stabilized Pickering emulsion was 3.14 ± 0.02 μm, which was smaller than that of the ZCP-stabilized emulsion. Compared with ZCPs, the rod-liked CNCs with a high aspect ratio could tangle with each other to form a bridge structure at the interface with a higher stability.[24] Madivala et al. (2009) found that the higher concentrations of particles could interconnect to form a triangular mesh structure, thus constituting the network of the emulsion and restricted the droplet coalescence.[38] Compared to ZCPs, elliptical particles (CNCs) showed a higher efficiency in stabilizing emulsions. Moreover, the adsorption rate of smaller CNCs was higher than larger ZCPs, although the smaller size simultaneously reduced the desorption energy of CNCs attached at the interface.[36,39]

When ZCPs and CNCs co-existed at the interface, the addition sequence and mass ratio of different particles exhibited significant influence on the droplet size. With the aid of CNCs, the droplet size of 4Z1C was decreased to 2.81 ± 0.11 μm (Fig. 2A). The presence of CNCs might reduce the hydrophobicity of ZCPs through adsorbing onto the particle surface, which might decrease the hydrophobic attraction between the droplets. Besides, Sarkar et al. (2018) proposed an idealized model of monodispersed spherical particles at its highest surface coverage on the droplet surface, the size of the interparticle gaps would be $\frac{(\sqrt{3}-1)d}{2} \approx 189.3\ nm$ for ZCPs of size $d = 517.3$ nm. This was much larger than the mean size of CNCs (115.2 nm) measured by DLS. The smaller CNCs could fill up the interfacial gaps, which was also evidenced by cryo-SEM (Fig. 10). The higher CNCs content increased the droplet size of Pickering emulsions. The CNCs in the outer layer of droplets could be connected to each other and resulted in droplet aggregation. On the contrary, in the Pickering emulsion with CNCs as an inner layer, the droplet size was decreased continuously with increasing the proportion of ZCPs. The CNCs were fixed at the interface along their length, which allowed their diffusion and reorganization. Therefore, a low concentration of CNCs was sufficient to cover the droplet surface of the emulsion and subsequently ZCPs could be adsorbed onto the CNCs-laden interface to provide extra steric hindrance. Excessive CNCs could scarcely adsorb onto the droplet surface adequately and instead stretch into the aqueous phase, causing the depletion flocculation, which was proved by the rheological properties of Pickering emulsions (Fig. 3B).

393 Fig. 2B shows the size distributions of Pickering emulsions stabilized by
394 individual ZCPs and CNCs as well as the complex interface with ZCPs as an inner
395 layer. The droplet size of the Pickering emulsion stabilized by ZCPs almost showed a
396 single peak distribution, while the size distribution of the Pickering emulsion
397 stabilized by CNCs showed a small peak below 1 μm. This result meant that at higher
398 particle concentrations, the wetting-induced self-assembly arose from CNCs in the
399 continuous phase with subsequent aggregation.[21] Similarly, in the emulsions
400 co-stabilized by whey protein and CNCs, the researchers revealed that unadsorbed
401 CNCs occurred in the continuous phase at the higher level, which was confirmed by
402 the droplet size distribution.[9] When the concentration of ZCPs in the inner layer was
403 low, the small peak with a droplet size less than 1 μm basically disappeared, but as the
404 concentration of ZCPs increased, the intensity of small peak gradually increased. This
405 phenomenon interpreted that at the lower mass ratio of ZCPs to CNCs, CNCs could
406 completely cover the surface of droplets. When the mass ratio of ZCPs to CNCs was
407 higher, ZCPs might self-associate to aggregate due to their hydrophobic attraction,
408 which was confirmed by the observation through CLSM (Fig. 9). Zhang et al. (2020)
409 reported the aggregation of unadsorbed particles in the continuous phase of the
410 emulsion stabilized by pea protein microgels due to the attraction between particles.[40]
411 A similar phenomenon was observed in Pickering emulsions stabilized by CNCs as an
412 inner layer (Fig. 2C). At the lower mass ratio of CNCs to ZCPs, the small peak less
413 than 1 μm appeared in the Pickering emulsion, indicating the aggregation of ZCPs in
414 the continuous phase. With increasing the mass ratio of CNCs to ZCPs, the large

particle aggregates gradually disappeared.

Fig. 2D demonstrates the zeta-potential of different emulsions. The Pickering emulsions stabilized by ZCPs and CNCs solely carried a large magnitude of positive and negative charges, respectively. Therefore, ZCPs and CNCs could form a layer-by-layer structure on the droplet surface by electrostatic deposition. With the increase in the mass ratio of ZCPs to CNCs, the absolute zeta-potential value was decreased slightly due to the electrostatic complexation of ZCPs and CNCs.

3.3. Rheological property

3.3.1. Apparent viscosity

The ZCP-stabilized Pickering emulsion showed the highest apparent viscosity among all the emulsions (Fig. 3A). As aforementioned, the interfacial particles (ZCPs) exhibited a strong hydrophobicity, which caused a serious droplet aggregation and even coalescence with the higher viscosity.[41] Besides, the CNC-stabilized Pickering emulsion showed a high viscosity, which was just behind the ZCPs. The wettability of particles is a key indicator indicating the propensity of an emulsion to aggregate via particle bridging. The hydrophilicity of CNCs promoted the particles entering the continuous phase, which decreased the attachment energy of particles and made them be shared between two droplets.[37] With the incorporation of CNCs into the ZCP-stabilized interface, the droplet size of Pickering emulsions with the particle-particle complex interface was decreased and the emulsion viscosity was also reduced greatly to a minimum (1Z1C). This phenomenon indicated that the addition

437 of CNCs improved the hydrophobicity of ZCPs to reduce particle bridges. The CNCs
438 were fully absorbed onto the interfacial gaps between ZCPs, and enhanced the
439 emulsion stability through strengthening the steric and electrostatic repulsion.
440 Nevertheless, the increasing proportion of CNCs gradually elevated the viscosity of
441 the emulsion. As aforementioned, CNCs preferentially formed particle bridges
442 between droplets due to their hydrophilicity. Additionally, excessive CNCs might
443 enter the continuous phase instead of adsorbing onto the interface, thus causing the
444 depletion flocculation.

445 When CNCs were applied as an inner layer, 1C4Z showed the highest viscosity
446 (Fig. 3B). This result was attributed to the hydrophobic interaction between ZCPs on
447 the outer layer, which caused the droplet aggregation and increased the emulsion
448 viscosity.[42] As the mass ratio of CNCs to ZCPs increased, the emulsion viscosity was
449 reduced rapidly to a minimum (1C2Z), interpreting that CNCs improved the stability
450 of the emulsions and the hydrophobic attraction between ZCPs was reduced. When
451 the proportion of CNCs was further increased, there was a continuous increase in the
452 viscosity of the emulsions. The high level of CNCs tended to form particle bridges
453 between droplets,[37] and entered the continuous phase to promote the depletion
454 flocculation.[46]

455 *3.3.2. Viscoelastic properties*

456 As illustrated in Fig. 3, the G' was higher than G" of all the Pickering emulsions,
457 suggesting that an elastic particulate gel-like structure was generated.[31] The G' value
458 of the Pickering emulsion stabilized by ZCPs or CNCs alone was maintained at a high

level (Fig. 3C). This result unraveled that ZCPs and CNCs tended to form particle bridges between droplets after adsorption at the interface induced by their strong hydrophobic interaction or hydrophilicity. The bridging flocculation between droplets increased the G' of the emulsions, exhibiting a solid-like behavior. With the adsorption of CNCs onto the ZCP-laden interface, the G' of 4Z1C was increased slightly compared with the ZCP-stabilized Pickering emulsion. Nevertheless, as the mass ratio of ZCPs to CNCs decreased, the viscoelasticity of Pickering emulsions with the particle-particle complex interface was reduced greatly and reached a minimum at 1Z1C. The presence of CNCs decreased the hydrophobicity of ZCPs and interfered with the bridging flocculation between droplets. As the proportion of CNCs continued to increase, the viscoelasticity of the emulsions increased again, revealing that the excessive CNCs located in the outer layer or dispersed into the continuous phase, thus promoting the depletion flocculation.

Fig. 3D depicts the viscoelasticity of the Pickering emulsion with CNCs as an inner layer. At the higher mass ratio of CNCs to ZCPs, the adsorption of CNCs saturated the droplet surface, and part of ZCPs entered the continuous phase to form larger aggregates. As the mass ratio of CNCs to ZCPs was decreased, the G' of the emulsions was reduced continuously to be close to the G", which revealed that the Pickering emulsions exhibited a transition from solid to liquid characteristics with decreasing the droplet size. The phenomenon proved that the combination of CNCs to ZCPs enhanced the repulsion between droplets through the interfacial layer and improved the emulsion stability synergistically. Notwithstanding, when the proportion

481 of ZCPs in the outer layer was further increased, the G' of the emulsion was greatly
482 increased due to the hydrophobic attraction between ZCPs, thereby leading to the
483 droplet flocculation.
484
485 *3.4. Environmental stability*
486 *3.4.1. Physical stability*
487 As depicted in Fig. 4A, the ZCP-stabilized Pickering emulsion showed the
488 highest instability index. Compared with ZCPs, the CNC-stabilized Pickering
489 emulsion showed a better physical stability. Similar to ZCPs, at the low CNCs
490 content, 4Z1C was more unstable compared to other Pickering emulsions with ZCPs
491 as an inner layer. With the mass ratio of ZCPs to CNCs decreasing, the emulsion
492 stability was improved until 1Z4C reached the minimum instability index. This result
493 suggested that ZCPs and CNCs could synergistically stabilize Pickering emulsions
494 with the complex interface, which was more stable than that of individual particle
495 stabilized-emulsions. As the proportion of CNCs increased, the emulsion stability
496 continued to be enhanced. Likewise, a similar phenomenon appeared in the physical
497 stability of Pickering emulsions with CNCs as an inner layer (Fig. 4B). Among all the
498 emulsions, 1C4Z showed the poorest physical stability due to the reduced electrostatic
499 repulsion and strong hydrophobic attraction between droplets. Nevertheless, the
500 higher mass ratio of CNCs to ZCPs enhanced the physical stability of emulsions. The
501 synergistic effect between CNCs and ZCPs was ascribed to that CNCs increased the
502 droplet surface coverage area and strengthened electrostatic repulsion. Meanwhile,

ZCPs could increase the steric repulsion against the droplet coalescence.

3.4.2. Photo stability

After 8 hours of light exposure, β-carotene in the ZCP-stabilized Pickering emulsion degraded most quickly (Fig. 5A), and the β-carotene content was reduced to 31.61 ± 2.24%. The large size of ZCPs made them unable to fully cover the droplet surface, so that more light could enter into the droplets through the interfacial gaps between particles, leading to the degradation of β-carotene.[8] The retention rate of β-carotene in the CNC-stabilized Pickering emulsion was elevated to 72.43 ± 0.67%. Compared to ZCPs, CNCs could form a more compact layer on the droplets, retarding the penetration of light and the degradation of β-carotene. It was observed that the introduction of the CNCs into polyvinyl alcohol films decreased their transparency with the strong anti-ultraviolet ability.[44] Similar to the physical stability of the emulsions, the complex interface could not protect β-carotene effectively at a lower CNCs concentration. For instance, the retention rate of β-carotene in 4Z1C was reduced to 53.20 ± 0.75%. As the mass ratio of CNCs to ZCPs increased, the photo stability of β-carotene in the droplets was gradually enhanced, indicating that CNCs could protect β-carotene from chemical degradation more effectively than ZCPs. Among all the emulsions, the retention rate of β-carotene in 1Z4C reached the maximum (80.43 ± 0.80%). Compared with a previous study, the Pickering emulsions co-stabilized by ZCPs and CNCs showed a better performance over the emulsions co-stabilized by zein-propylene glycol alginate (PGA) composite nanoparticles and lactoferrin or rhamnolipid in the protection of β-carotene against UV radiation.[8] This

phenomenon interpreted that the mixed particles-constituting interface could provide a better protection for bioactive compounds under the exposure of light than that adsorbed by individual particles and emulsifiers or their combinations.

3.4.3. Thermal stability

The droplet size of the ZCP-stabilized Pickering emulsion was increased greatly to 115.37 ± 7.52 μm after thermal treatment (Fig. 5B), revealing that the thermal treatment induced the droplet coalescence.[42] Thermal treatment denatured the interfacial protein with the exposure of hydrophobic groups, which promoted the aggregation between the interfacial particles. Conversely, the CNC-stabilized Pickering emulsion remained stable after thermal treatment with a constant droplet size, indicating that the introduction of CNCs endowed the interface with a great thermal resistance owing to the stable structure of CNCs.[44] With the complexation of ZCPs and CNCs, there was an obvious increase in the droplet size of Pickering emulsions at the low level of CNCs. As the proportion of CNCs was elevated, the thermal stability of Pickering emulsions was improved, regardless of the order of addition of ZCPs and CNCs. The zeta-potential was decreased slightly after thermal treatment, indicating that part of the particles desorbed from the interface. The absolute zeta-potential value of emulsion droplets was positively correlated with the degree of emulsion aggregation (Fig. 5C), which suggested that electrostatic repulsion exerted an important role in the stabilization of Pickering emulsions.

After incubated at 90 ℃ for 60 min, β-carotene in the ZCP-stabilized Pickering emulsion showed the lowest retention rate (18.03 ± 0.92%) (Fig. 5D). The

CNC-stabilized Pickering emulsion showed a much better protection for β-carotene (76.72 ± 0.58%) against thermal degradation due to the outstanding thermal stability of CNCs compared to protein nanoparticles.[44] Owing to the high aspect ratio, the CNCs might form a more compact interfacial layer with less gaps at the interface to reduce the transmit of heat. Through forming the particle-particle complex interface, the thermal stability of β-carotene entrapped was further enhanced, except at the high ratio of ZCPs to CNCs. This phenomenon revealed the synergistic effect of ZCPs and CNCs in strengthening the thermal stability of Pickering emulsions.

3.4.4. Storage stability

The storage stability of Pickering emulsions was tested for 4 weeks and the size fluctuation of Pickering emulsions is demonstrated in Fig. 6A. The ZCP-stabilized Pickering emulsion showed the largest increase of droplet size and was followed by 4Z1C and 1C4Z. Compared with ZCPs, the CNC-stabilized Pickering emulsion showed better storage stability with a small increase of droplet size. With the continuous increase in CNC concentration, the storage stability of Pickering emulsions with the mixed particle-particle interface was greatly improved. These results confirmed that the layer-by-layer structure of ZCPs and CNCs endowed the droplets with a rigid and robust interface to prevent the emulsion coalescence, and therefore different types of particles could synergistically stabilize the emulsions.

The chemical stability of β-carotene loaded in the emulsions was investigated during a long-term storage (Fig. 6B). The β-carotene in the ZCP-stabilized Pickering emulsion was the most unstable, with retention rates of 32.13 ± 0.78% and 9.29 ±

569 1.24% after 7 and 28 days, respectively. The β-carotene in the CNC-stabilized
570 Pickering emulsion showed a better stability, with 94.24 ± 0.56% and 54.69 ± 2.89%
571 remaining after 7 and 28 days, respectively. However, the storage stability of
572 β-carotene in the Pickering emulsion co-stabilized by ZCPs and CNCs was not
573 improved compared with the CNC-stabilized Pickering emulsion. With the mass ratio
574 of CNCs to ZCPs rising, the retention rate of β-carotene slightly increased, reaching
575 the maximum in 1Z4C, manifesting that CNCs exerted a more important role in
576 protecting β-carotene against chemical degradation through forming a denser
577 interfacial layer.

578 *3.4.5. pH stability*

579 The impact of different pHs on the stability of Pickering emulsions with the
580 particle-particle mixed interface was investigated (Fig. 7). All of the emulsions
581 remained stable at pH 2.0 except CNCs. The droplet size of the CNC-stabilized
582 Pickering emulsion was increased slightly due to the reduced electrostatic repulsion.
583 With the pH being adjusted to 6, the droplet size of the ZCP-stabilized Pickering
584 emulsion mostly increased, which was due to the pH close to the pI of zein. Other
585 emulsions exhibited a good stability at pH 6.0 except 4Z1C, presumable for the same
586 reason. In a pH neutral environment, the bilayered interfacial structure consisting of
587 ZCPs and CNCs provided the sufficient steric and electrostatic repulsion. The droplet
588 size of the Pickering emulsion solely stabilized by ZCPs was decreased obviously
589 when pH was elevated from 6 to 9. The increased charge strengthened the
590 electrostatic repulsion between droplets. Although both ZCPs and CNCs carried

591 negative charges and repelled each other, the Pickering emulsion with the
592 particle-particle complex interface kept stable, which showed that the layer-by-layer
593 interfacial structure composed of different particles was more stable than
594 particle-biopolymer or particle-surfactant complex interfaces developed from our
595 laboratory.[8,32] This phenomenon was mainly explained by that when the attraction
596 between particle and biopolymer was not strong enough, the biopolymer could diffuse
597 into the continuous phase, leading to depletion flocculation between droplets.[30,45,46]

598 *3.4.6. Ionic strength stability*

599 The stability of Pickering emulsions was explored at different ionic strengths.
600 The droplet sizes of all emulsions remained stable at 50 mM (Fig. 8). Increasing NaCl
601 concentration to 100 mM obviously increased the droplet size of the ZCP-stabilized
602 Pickering emulsion due to the reduced electrostatic repulsion. Particularly, the droplet
603 sizes of the CNC-stabilized Pickering emulsion and other emulsions with the mixed
604 particle-particle interfaces were decreased slightly at higher ionic strengths. This
605 result may be attributed to that electrostatic shielding weakened the repulsion between
606 CNCs, thereby promoting the adsorption of CNCs onto the interface.[24,47] When the
607 ionic strength was increased to 200 mM, the droplet sizes of most emulsions were
608 increased slightly due to the reduced electrostatic repulsion. It is noteworthy that a
609 larger increase of the droplet size appeared in ZCPs and 4Z1C, indicating that the
610 Pickering emulsions were more unstable at a higher level of ZCPs. This phenomenon
611 showed that it was difficult for ZCPs alone or the interfacial layer dominated by ZCPs
612 to stabilize the Pickering emulsion at a higher ionic strength. As the electrostatic

repulsion between droplets was reduced, the hydrophobic attraction between particles induced the droplet flocculation. Nevertheless, at the higher proportion of CNCs, ZCPs and CNCs exhibited a synergistic effect in stabilizing Pickering emulsions.

3.5. Morphological observation

The droplets of the ZCP-stabilized Pickering emulsion were severely flocculated and bridged by ZCPs and their aggregates (Fig. 9). In contrast, in the CNC-stabilized Pickering emulsion, the droplets were individually separated from each other without aggregation, indicating that CNCs were densely packed onto the droplet surface and provided the additional steric and electrostatic repulsion against the emulsion coalescence. When ZCPs were used as an inner layer and CNCs as an outer layer, a slight decrease appeared in the droplet size of Pickering emulsions with the particle-particle mixed interface at higher CNCs levels. Besides, the "red" ZCPs could not be observed at the interface through CLSM at a higher CNCs level, which suggested that CNCs displaced the part of ZCPs from the droplet surface. With the mass ratio of ZCPs to CNCs rising, there was an obvious aggregation in the emulsions with larger droplet sizes. It was observed that ZCPs began to adsorb on the interface and aggregate, and even enter the continuous phase, which was consistent with the size distributions of Pickering emulsions (Fig. 2B). This phenomenon indicated that ZCPs aggregated with each other into larger particle aggregates due to hydrophobic interaction, reducing the efficiency of covering on the interface. Meanwhile, a higher proportion of ZCPs could generate more bridges between droplets, further forming a

network structure.

When CNCs were utilized as an inner layer, it was hard to distinguish the protein particle layer on the droplet surface (Fig. 9). Alternatively, when the proportion of ZCPs was high, hydrophobic ZCPs aggregated into larger clusters in the continuous phase, which might cause the depletion flocculation. With the rise of CNCs proportion, the droplet size of Pickering emulsions decreased and then increased slightly. This result showed that when rod-shaped CNCs were fully adsorbed on the droplet surface, they could provide sufficient steric and electrostatic repulsion to retard coalescence. At the higher mass ratio of CNCs to ZCPs, excessive CNCs might enter the continuous phase, inducing depletion flocculation between droplets.[24,47]

Cryo-SEM can be applied to observe the microstructure of Pickering emulsions with the mixed particle-particle interface (Fig. 10), which allows it to complement each other with CLSM. The distribution of ZCPs on the droplet surface was obviously sparse and they could not occupy the droplet surface adequately and prevent the droplet aggregation. Additionally, due to the larger size and strong hydrophobicity, ZCPs tended to aggregate and bridge in the interfacial or the bulk phase, which reduced the packing efficiency of the particles on the droplet surface. Compared to the ZCP-stabilized Pickering emulsion, the rod-shaped CNCs were densely distributed at the interface to form a rigid layer, inhibiting coalescence more efficiently. With the complexation of ZCPs and CNCs, it was observed that loosely distributed ZCPs with a larger size and closely packed CNCs with a smaller size were co-adsorbed at the interface. At a lower proportion of ZCPs, a small amount of ZCPs was sparsely

dispersed on the droplet surface, while densely distributed CNCs could be observed on the rest of the droplet surface. As the level of ZCPs increased, more and larger ZCPs with uneven particle size would appear, indicating that ZCPs tended to aggregate at the interface due to the strong hydrophobicity. The phenomenon was consistent with the observation through CLSM. It is worth noting that CNCs could be adsorbed to the surface of ZCPs aggregates, which might change the properties of the interfacial particles. Regardless of the addition sequence, the effect of the mass ratio of ZCPs and CNCs on the interfacial structure was basically consistent.

3.6. In vitro digestion of Pickering emulsions

3.6.1. Lipid digestion

As depicted in Fig. 11A, the ZCP-stabilized Pickering emulsion showed the highest FFA release (19.46%), though it was lower than traditional emulsions stabilized by biopolymers or surfactants.[10] Meanwhile, the CNC-stabilized Pickering emulsion showed a much lower FFA release (12.31%). The particle stabilizers were difficult to be displaced by bile salts or lipases due to the high desorption energy, which could restrict the lipid digestion efficiently. Nevertheless, in this study, ZCPs could hardly cover the interface adequately due to the particle aggregation, and therefore there existed substantial interfacial gaps between ZCPs.[8] The cryo-SEM images showed the droplets surrounded by a compact layer of CNCs, demonstrating the propensity of the CNCs to restrict the contact of bile salts and lipases/co-lipases

678 with the droplet surface (Fig. 10). These results suggested that compared with the
679 protein particles that were easily affected by enzymes conditions, CNCs were more
680 promising as Pickering emulsion stabilizers in controlling the lipid digestion.[24] As a
681 control, the MCT oil was digested under the GIT, which only released 5.38% FFA in
682 the intestinal phase. Without the addition of effective emulsifiers, the triglycerides
683 were not dispersed and stabilized before entering the GIT, which reduced the specific
684 surface area of the lipid phase and limited the contact of droplets with lipases.

685 With the incorporation of CNCs, the lipolysis of the ZCP-stabilized Pickering
686 emulsion was effectively retarded. The FFA release rate of 4Z1C was reduced to
687 12.88% at a low proportion of CNCs. CNCs could enter into the uncovered areas in
688 the ZCP-stabilized interface, which blocked the gaps at the ZCP-coated interface and
689 limited the access of bile salts and lipases to the interface.[48] With the continuous
690 increase in CNCs proportion, the FFA release of Pickering emulsions was slightly
691 decreased and similar to the CNC-stabilized interface. In addition to the adsorption
692 onto the gaps between ZCPs at the interface, excessive CNCs could combine with
693 ZCPs and cover the surface of ZCPs through electrostatic and hydrophobic attraction,
694 which limited the proteolysis and detachment of protein particles. As the outer layer,
695 CNCs adsorbed to the droplet surface also reduced the proximity of the negatively
696 charged bile salts and lipase through charge repulsion, which restricted the interfacial
697 displacement. It was reported the bridging of CNCs to the protein-covered droplets
698 could reduce the exposed surface area of the droplets for lipid digestion.[9]

When CNCs were utilized as an inner layer, the FFA release of Pickering emulsions with the particle-particle complex interfaces was much lower than that with ZCPs as the inner layer. Compared with the Pickering emulsion stabilized by CNCs alone, as the proportion of ZCPs was elevated, the degree of lipid hydrolysis of the emulsions was gradually decreased. The continuous rise of ZCPs reduced the release rate of FFA to 11.36%, 9.08%, and 8.73% for 4C1Z, 1C1Z, and 1C4Z, respectively. Compared with the ZCP-stabilized interface, the irreversibly strong adsorption of CNCs onto the droplet surface restricted the penetration of bile salts and lipases more effectively owing to the formation of a densely packed shell with CNCs as an inner layer. Nevertheless, it was at odds with previous studies on the CNC-stabilized Pickering emulsion, which reported that the degree of inhibiting the lipolysis was improved with the increase of CNCs concentration. Interestingly, in this case, decreasing the mass ratio of CNCs to ZCPs strengthened the ability of complex interfaces in retarding lipolysis, indicating that CNCs and ZCPs could synergistically delay the lipid digestion. This phenomenon could be explained by the positive charge of ZCPs, which could produce strong electrostatic complexation between ZCPs and negatively charged bile salts, thereby reducing the approaching and displacement of bile salts at the interface. The CLSM images showed that the addition of ZCPs as an outer layer caused droplet flocculation in Pickering emulsions (Fig. 9). The relatively large droplet size (low specific surface area) reduced the exposed surface area accessible to bile salts. Moreover, the higher viscosity limited the diffuse and adsorption of bile salts and lipase/co-lipase and delayed the digestion (Fig. 3B).[41,49]

721 *3.6.2. Bioaccessibility of β-carotene*

722 As a prerequisite for determining the bioaccessibilities, the release and
723 solubilization of fat-soluble nutrients mainly occur in the digestion stage of the small
724 intestine and are dependent on a variety of exogenous factors, such as molecular
725 property, food matrix, processing, and interfacial composition.[50] In the present study,
726 the β-carotene bioaccessibility of the ZCP-stabilized emulsion was 27.25% and
727 significantly higher than those of other emulsions (Fig. 11B), which was consistent
728 with its highest FFA release. Substances such as FFAs and bile salts facilitated the
729 formation of mixed micelles, and lipolysis promoted the ability of mixed micelles to
730 dissolve nutrients. Meanwhile, indigestible CNCs formed a densely packed interface
731 that restricted the access of bile salts and lipases to lipid droplets, which effectively
732 reduced the FFA release and β-carotene bioaccessibility (20.14%). As a control, the
733 unemulsified oil containing β-carotene was mixed with simulated small intestine
734 fluids and the lowest β-carotene bioaccessibility was found in MCT (4.56%). In the
735 absence of exogenous emulsifiers, the bile salts were incapable of stabilizing
736 emulsions, thus causing the droplet flocculation and coalescence. The large droplet
737 size resulted in low specific surface area available for lipase/co-lipase attachment,
738 which inhibited the FFA release and decreased the β-carotene bioaccessibility. The
739 interfacial composition exhibited a profound influence on the Pickering emulsions
740 with the particle-particle composite interface. When ZCPs were used as an inner layer
741 and CNCs as an outer layer, the bioaccessibility of β-carotene was continuously
742 reduced with increase in the CNCs proportion. This result was mainly because CNCs

743 could fill the interfacial gaps in ZCPs-covered droplets and limit the access of bile
744 salts and lipases to reach the droplet surface.[48] Besides, CNCs adsorbed limited the
745 proximity of the negatively charged bile salts and lipase through charge repulsion.
746 The declination in the FFA release consequently reduced the formation of mixed
747 micelles and the transfer of nutrients. Meanwhile, the addition of ZCPs onto the
748 CNCs-stabilized emulsion decreased the bioaccessibility of β-carotene from 20.13%
749 (4C1Z) to 9.14% (1C4Z). This result could be attributed to that the negatively charged
750 ZCPs strengthened repulsion to negatively charged bile salts at the neutural pH under
751 the intestinal condition, which not only restricted the approaching of bile salts at the
752 interface, but also reduced the participation of bile salts in forming mixed micelles.
753 These mechanisms explained the lower bioaccessibility of β-carotene in the Pickering
754 emulsions with CNCs as the inner layer and ZCPs as the outer layer, and the
755 bioaccessibility of β-carotene was increased with the decrease in the level of ZCPs.

756

757 **4. Conclusion**

758 Spherical hydrophobic ZCPs and rod-shaped hydrophilic CNCs were combined
759 to stabilize Pickering emulsions for delivery of β-carotene. Through the layer-by-layer
760 deposition method, the physicochemical stability of Pickering emulsions was tailored
761 through adjusting the mass ratio and addition sequence of different particles. Among
762 all the emulsions, when the mass ratio of ZCPs to CNCs was 1:4, the Pickering
763 emulsions with the particle-particle complex interface showed the best stability.
764 Meanwhile, when CNCs was an inner layer and ZCPs was an outer layer, they could

765 synergistically inhibit the lipolysis of Pickering emulsions in gastrointestinal digestion
766 through steric and electrostatic interaction while maintaining a higher bioaccessibility
767 of β-carotene. The experimental results confirmed that the retardance of fat digestion
768 was most profound when CNCs were used as the inner layer. The novel Pickering
769 emulsion with the particle-particle complex interface could be incorporated in foods
770 as well as pharmaceuticals for inhibition of lipid hydrolysis or precise delivery of
771 nutraceuticals.

ASSOCIATED CONTENT

AUTHOR INFORMATION

Corresponding Author

*E-mail: gyxcau@126.com

Notes

The authors declare no competing financial interest.

Acknowledgement

The research was funded by the National Natural Science Foundation of China (No. 31871842). The authors are grateful to Tsinghua University Branch of China National Center Protein Sciences (Beijing, China) for providing the facility support of Cryo-SEM with the aid of Xiaomin Li.

References:

772 (1) P. Binks, B.; O. Lumsdon, S. Influence of Particle Wettability on the Type and
773 Stability of Surfactant-Free Emulsions. *Langmuir* **2000**, *16* (23), 8622–8631.

774 https://doi.org/10.1021/la000189s.

775 (2) Xiao, J.; Li, Y.; Huang, Q. Recent Advances on Food-Grade Particles
776 Stabilized Pickering Emulsions: Fabrication, Characterization and Research
777 Trends. *Trends Food Sci. Technol.* **2016**, *55*, 48–60.
778 https://doi.org/10.1016/J.TIFS.2016.05.010.

779 (3) Zou, Y.; Guo, J.; Yin, S.-W.; Wang, J.-M.; Yang, X.-Q. Pickering Emulsion
780 Gels Prepared by Hydrogen-Bonded Zein/Tannic Acid Complex Colloidal
781 Particles. *J. Agric. Food Chem.* **2015**, *63* (33), 7405–7414.
782 https://doi.org/10.1021/acs.jafc.5b03113.

783 (4) Wei, Y.; Yu, Z.; Lin, K.; Yang, S.; Tai, K.; Liu, J.; Mao, L.; Yuan, F.; Gao, Y.
784 Fabrication, Physicochemical Stability, and Microstructure of Coenzyme Q10
785 Pickering Emulsions Stabilized by Resveratrol-Loaded Composite
786 Nanoparticles. *J. Agric. Food Chem.* **2020**, *68* (5), 1405–1418.
787 https://doi.org/10.1021/acs.jafc.9b06678.

788 (5) Binks, B. P.; Desforges, A.; Duff, D. G. Synergistic Stabilization of Emulsions
789 by a Mixture of Surface-Active Nanoparticles and Surfactant. *Langmuir* **2007**,
790 *23* (3), 1098–1106. https://doi.org/10.1021/la062510y.

791 (6) Dickinson, E. Mixed Biopolymers at Interfaces: Competitive Adsorption and
792 Multilayer Structures. *Food Hydrocoll.* **2011**, *25* (8), 1966–1983.
793 https://doi.org/10.1016/J.FOODHYD.2010.12.001.

794 (7) McClements, D. J.; Gumus, C. E. Natural Emulsifiers — Biosurfactants,
795 Phospholipids, Biopolymers, and Colloidal Particles: Molecular and

796 Physicochemical Basis of Functional Performance. *Adv. Colloid Interface Sci.*
797 **2016**, *234*, 3–26. https://doi.org/10.1016/j.cis.2016.03.002.
798 (8) Wei, Y.; Tong, Z.; Dai, L.; Wang, D.; Lv, P.; Liu, J.; Mao, L.; Yuan, F.
799 Influence of Interfacial Compositions on the Microstructure , Physiochemical
800 Stability , Lipid Digestion and β -Carotene Bioaccessibility of Pickering
801 Emulsions. *Food Hydrocoll.* **2020**, *104* (17), 105738.
802 https://doi.org/10.1016/j.foodhyd.2020.105738.
803 (9) Sarkar, A.; Li, H.; Cray, D.; Boxall, S. Composite Whey Protein–Cellulose
804 Nanocrystals at Oil-Water Interface: Towards Delaying Lipid Digestion. *Food*
805 *Hydrocoll.* **2018**, *77*, 436–444. https://doi.org/10.1016/j.foodhyd.2017.10.020.
806 (10) Sarkar, A.; Zhang, S.; Holmes, M.; Ettelaie, R. Colloidal Aspects of Digestion
807 of Pickering Emulsions: Experiments and Theoretical Models of Lipid
808 Digestion Kinetics. *Advances in Colloid and Interface Science*. Elsevier B.V.
809 January 1, 2019, pp 195–211. https://doi.org/10.1016/j.cis.2018.10.002.
810 (11) Sarkar, A.; Ademuyiwa, V.; Stubley, S.; Esa, N. H.; Goycoolea, F. M.; Qin, X.;
811 Gonzalez, F.; Olvera, C. Pickering Emulsions Co-Stabilized by Composite
812 Protein/ Polysaccharide Particle-Particle Interfaces: Impact on in Vitro Gastric
813 Stability. *Food Hydrocoll.* **2018**, *84* (June), 282–291.
814 https://doi.org/10.1016/j.foodhyd.2018.06.019.
815 (12) Eric, D. *Colloidal Particles at Liquid Interfaces: Interfacial Particles in Food*
816 *Emulsions and Foams*; Cambridge University Press: Cambridge, 2006.
817 (13) Shi, A.; Feng, X.; Wang, Q.; Adhikari, B. Pickering and High Internal Phase

818 Pickering Emulsions Stabilized by Protein-Based Particles: A Review of
819 Synthesis, Application and Prospective. *Food Hydrocoll.* **2020**, 106117.
820 https://doi.org/10.1016/j.foodhyd.2020.106117.
821 (14) Hu, Z.; Ballinger, S.; Pelton, R.; Cranston, E. D. Surfactant-Enhanced
822 Cellulose Nanocrystal Pickering Emulsions. *J. Colloid Interface Sci.* **2015**, *439*,
823 139–148. https://doi.org/10.1016/j.jcis.2014.10.034.
824 (15) Beck-Candanedo, S.; Roman, M.; Gray, D. G. Effect of Reaction Conditions on
825 the Properties and Behavior of Wood Cellulose Nanocrystal Suspensions.
826 *Biomacromolecules* **2005**, *6* (2), 1048–1054.
827 https://doi.org/10.1021/bm049300p.
828 (16) Klemm, D.; Kramer, F.; Moritz, S.; Lindström, T.; Ankerfors, M.; Gray, D.;
829 Dorris, A. Nanocelluloses: A New Family of Nature-Based Materials. *Angew.*
830 *Chemie - Int. Ed.* **2011**, *50* (24), 5438–5466.
831 https://doi.org/10.1002/anie.201001273.
832 (17) Moon, R. J.; Martini, A.; Nairn, J.; Simonsen, J.; Youngblood, J. *Cellulose*
833 *Nanomaterials Review: Structure, Properties and Nanocomposites*; 2011; Vol.
834 40. https://doi.org/10.1039/c0cs00108b.
835 (18) Hu, Z.; Patten, T.; Pelton, R.; Cranston, E. D. Synergistic Stabilization of
836 Emulsions and Emulsion Gels with Water-Soluble Polymers and Cellulose
837 Nanocrystals. *ACS Sustain. Chem. Eng.* **2015**, *3* (5), 1023–1031.
838 https://doi.org/10.1021/acssuschemeng.5b00194.
839 (19) Kalashnikova, I.; Bizot, H.; Cathala, B.; Capron, I. Modulation of Cellulose

840 Nanocrystals Amphiphilic Properties to Stabilize Oil/Water Interface.
841 *Biomacromolecules* **2012**, *13* (1), 267–275. https://doi.org/10.1021/bm201599j.
842 (20) Kalashnikova, I.; Bizot, H.; Bertoncini, P.; Cathala, B.; Capron, I. Cellulosic
843 Nanorods of Various Aspect Ratios for Oil in Water Pickering Emulsions. *Soft*
844 *Matter* **2013**, *9* (3), 952–959. https://doi.org/10.1039/c2sm26472b.
845 (21) Capron, I.; Cathala, B. Surfactant-Free High Internal Phase Emulsions
846 Stabilized by Cellulose Nanocrystals. *Biomacromolecules* **2013**, *14* (2), 291–
847 296. https://doi.org/10.1021/bm301871k.
848 (22) Li, X.; Li, J.; Gong, J.; Kuang, Y.; Mo, L.; Song, T. Cellulose Nanocrystals
849 (CNCs) with Different Crystalline Allomorph for Oil in Water Pickering
850 Emulsions. *Carbohydr. Polym.* **2018**, *183* (January), 303–310.
851 https://doi.org/10.1016/j.carbpol.2017.12.085.
852 (23) Capron, I.; Rojas, O. J.; Bordes, R. Behavior of Nanocelluloses at Interfaces.
853 *Curr. Opin. Colloid Interface Sci.* **2017**, *29*, 83–95.
854 https://doi.org/10.1016/j.cocis.2017.04.001.
855 (24) Dai, H.; Wu, J.; Zhang, H.; Chen, Y.; Ma, L.; Huang, H.; Huang, Y.; Zhang, Y.
856 Recent Advances on Cellulose Nanocrystals for Pickering Emulsions:
857 Development and Challenge. *Trends Food Sci. Technol.* **2020**, *102* (2), 16–29.
858 https://doi.org/10.1016/j.tifs.2020.05.016.
859 (25) Patel, A. R.; Velikov, K. P. Zein as a Source of Functional Colloidal Nano- and
860 Microstructures. *Curr. Opin. Colloid Interface Sci.* **2014**, *19* (5), 450–458.
861 https://doi.org/10.1016/J.COCIS.2014.08.001.

862 (26) De Folter, J. W. J.; Van Ruijven, M. W. M.; Velikov, K. P. Oil-in-Water
863 Pickering Emulsions Stabilized by Colloidal Particles from the Water-Insoluble
864 Protein Zein. *Soft Matter* **2012**, *8* (25), 6807–6815.
865 https://doi.org/10.1039/c2sm07417f.
866 (27) Dai, L.; Sun, C.; Wei, Y.; Mao, L.; Gao, Y. Characterization of Pickering
867 Emulsion Gels Stabilized by Zein/Gum Arabic Complex Colloidal
868 Nanoparticles. *Food Hydrocoll.* **2018**, *74*, 239–248.
869 https://doi.org/10.1016/J.FOODHYD.2017.07.040.
870 (28) Wei, Y.; Yu, Z.; Lin, K.; Yang, S.; Tai, K.; Liu, J.; Mao, L.; Yuan, F.; Gao, Y.
871 Fabrication, Physicochemical Stability and Microstructure of Coenzyme Q10
872 Pickering Emulsions Stabilized by Resveratrol Loaded Composite
873 Nanoparticles. *J. Agric. Food Chem.* **2020**, *0* (ja).
874 https://doi.org/10.1021/acs.jafc.9b06678.
875 (29) Wei, Y.; Sun, C.; Dai, L.; Zhan, X.; Gao, Y. Structure, Physicochemical
876 Stability and in Vitro Simulated Gastrointestinal Digestion Properties of
877 β-Carotene Loaded Zein-Propylene Glycol Alginate Composite Nanoparticles
878 Fabricated by Emulsification-Evaporation Method. *Food Hydrocoll.* **2018**, *81*,
879 149–158. https://doi.org/10.1016/j.foodhyd.2018.02.042.
880 (30) Wei, Y.; Zhou, D.; Mackie, A.; Yang, S.; Dai, L.; Zhang, L.; Mao, L.; Gao, Y.
881 Stability, Interfacial Structure, and Gastrointestinal Digestion of
882 β-Carotene-Loaded Pickering Emulsions Co-Stabilized by Particles, a
883 Biopolymer, and a Surfactant. *J. Agric. Food Chem.* **2021**, *69* (5), 1619–1636.

884 https://doi.org/10.1021/acs.jafc.0c06409.

885 (31) Wei, Y.; Sun, C.; Dai, L.; Mao, L.; Yuan, F.; Gao, Y. Novel Bilayer Emulsions
886 Costabilized by Zein Colloidal Particles and Propylene Glycol Alginate. 2.
887 Influence of Environmental Stresses on Stability and Rheological Properties. *J.*
888 *Agric. Food Chem.* **2019**, *67* (4), 1209–1221.
889 https://doi.org/10.1021/acs.jafc.8b04994.

890 (32) Wei, Y.; Tong, Z.; Dai, L.; Ma, P.; Zhang, M.; Liu, J.; Mao, L.; Yuan, F.; Gao,
891 Y. Novel Colloidal Particles and Natural Small Molecular Surfactants
892 Co-Stabilized Pickering Emulsions with Hierarchical Interfacial Structure:
893 Enhanced Stability and Controllable Lipolysis. *J. Colloid Interface Sci.* **2020**,
894 *563*, 291–307. https://doi.org/10.1016/J.JCIS.2019.12.085.

895 (33) Sriamornsak, P.; Thirawong, N.; Cheewatanakornkool, K.; Burapapadh, K.;
896 Sae-Ngow, W. Cryo-Scanning Electron Microscopy (Cryo-SEM) as a Tool for
897 Studying the Ultrastructure during Bead Formation by Ionotropic Gelation of
898 Calcium Pectinate. *Int. J. Pharm.* **2008**, *352* (1–2), 115–122.
899 https://doi.org/10.1016/J.IJPHARM.2007.10.038.

900 (34) Li, Y.; McClements, D. J. Inhibition of Lipase-Catalyzed Hydrolysis of
901 Emulsified Triglyceride Oils by Low-Molecular Weight Surfactants under
902 Simulated Gastrointestinal Conditions. *Eur. J. Pharm. Biopharm.* **2011**, *79* (2),
903 423–431. https://doi.org/10.1016/j.ejpb.2011.03.019.

904 (35) Li, Y.; Julian McClements, D. New Mathematical Model for Interpreting
905 PH-Stat Digestion Profiles: Impact of Lipid Droplet Characteristics on in Vitro

906 Digestibility. *J. Agric. Food Chem.* **2010**, *58* (13), 8085–8092.
907 https://doi.org/10.1021/jf101325m.
908 (36) Binks, B. P. Particles as Surfactants—Similarities and Differences. *Curr. Opin.*
909 *Colloid Interface Sci.* **2002**, *7* (1–2), 21–41.
910 https://doi.org/10.1016/S1359-0294(02)00008-0.
911 (37) French, D. J.; Taylor, P.; Fowler, J.; Clegg, P. S. Making and Breaking Bridges
912 in a Pickering Emulsion. *J. Colloid Interface Sci.* **2015**, *441*, 30–38.
913 https://doi.org/10.1016/J.JCIS.2014.11.032.
914 (38) Madivala, B.; Fransaer, J.; Vermant, J. Self-Assembly and Rheology of
915 Ellipsoidal Particles at Interfaces. *Langmuir* **2009**, *25* (5), 2718–2728.
916 https://doi.org/10.1021/la803554u.
917 (39) Wu, J.; Ma, G. H. Recent Studies of Pickering Emulsions: Particles Make the
918 Difference. *Small* **2016**, *12* (34), 4633–4648.
919 https://doi.org/10.1002/smll.201600877.
920 (40) Zhang, S.; Holmes, M.; Ettelaie, R.; Sarkar, A. Pea Protein Microgel Particles
921 as Pickering Stabilisers of Oil-in-Water Emulsions: Responsiveness to PH and
922 Ionic Strength. *Food Hydrocoll.* **2020**.
923 https://doi.org/10.1016/j.foodhyd.2019.105583.
924 (41) MacKie, A.; Gourcy, S.; Rigby, N.; Moffat, J.; Capron, I.; Bajka, B. The Fate
925 of Cellulose Nanocrystal Stabilised Emulsions after Simulated Gastrointestinal
926 Digestion and Exposure to Intestinal Mucosa. *Nanoscale* **2019**, *11* (6), 2991–
927 2998. https://doi.org/10.1039/c8nr05860a.

928 (42) Wei, Y.; Sun, C.; Dai, L.; Mao, L.; Yuan, F.; Gao, Y. Novel Bilayer Emulsions
929 Costabilized by Zein Colloidal Particles and Propylene Glycol Alginate, Part 1:
930 Fabrication and Characterization. *J. Agric. Food Chem.* **2019**, *67* (4), 1197–
931 1208. https://doi.org/10.1021/acs.jafc.8b03240.
932 (43) Dickinson, E. Biopolymer-Based Particles as Stabilizing Agents for Emulsions
933 and Foams. *Food Hydrocoll.* **2017**, *68*, 219–231.
934 https://doi.org/10.1016/J.FOODHYD.2016.06.024.
935 (44) Dai, H.; Huang, Y.; Huang, H. Enhanced Performances of Polyvinyl Alcohol
936 Films by Introducing Tannic Acid and Pineapple Peel-Derived Cellulose
937 Nanocrystals. *Cellulose* **2018**, *25* (8), 4623–4637.
938 https://doi.org/10.1007/s10570-018-1873-5.
939 (45) Dickinson, E. Mixed Biopolymers at Interfaces: Competitive Adsorption and
940 Multilayer Structures. *Food Hydrocoll.* **2011**, *25* (8), 1966–1983.
941 https://doi.org/10.1016/j.foodhyd.2010.12.001.
942 (46) Wei, Y.; Zhou, D.; Yang, S.; Dai, L.; Zhang, L.; Mao, L. Development of
943 β-Carotene Loaded Oil-in-Water Emulsions Using Mixed Biopolymer–
944 Particle– Development of β-Carotene Loaded Oil-in-Water Surfactant
945 Interfaces. *Food Funct.* **2021**, No. 2009. https://doi.org/10.1039/d0fo02975k.
946 (47) Bai, L.; Lv, S.; Xiang, W.; Huan, S.; McClements, D. J.; Rojas, O. J.
947 Oil-in-Water Pickering Emulsions via Microfluidization with Cellulose
948 Nanocrystals: 1. Formation and Stability. *Food Hydrocoll.* **2019**, *96* (April),
949 699–708. https://doi.org/10.1016/j.foodhyd.2019.04.038.

950 (48) Bai, L.; Lv, S.; Xiang, W.; Huan, S.; McClements, D. J.; Rojas, O. J.
951 Oil-in-Water Pickering Emulsions via Microfluidization with Cellulose
952 Nanocrystals: 1. Formation and Stability. *Food Hydrocoll.* **2019**, *96* (January),
953 699–708. https://doi.org/10.1016/j.foodhyd.2019.04.038.
954 (49) Bai, L.; Lv, S.; Xiang, W.; Huan, S.; McClements, D. J.; Rojas, O. J.
955 Oil-in-Water Pickering Emulsions via Microfluidization with Cellulose
956 Nanocrystals: 2. In Vitro Lipid Digestion. *Food Hydrocoll.* **2019**, *96* (April),
957 709–716. https://doi.org/10.1016/j.foodhyd.2019.04.039.
958 (50) Dima, C.; Assadpour, E.; Dima, S.; Jafari, S. M. Bioavailability of
959 Nutraceuticals: Role of the Food Matrix, Processing Conditions, the
960 Gastrointestinal Tract, and Nanodelivery Systems. *Compr. Rev. Food Sci. Food*
961 *Saf.* **2020**, No. January, 1–41. https://doi.org/10.1111/1541-4337.12547.

Figure captions

Fig. 1 TEM images of ZCPs (A) and CNCs (B); AFM image of CNCs (C); TEM image of ZCPs-CNCs mixtures (D); wettabilities of ZCPs (E) and CNCs (F);

Fig. 2 Mean droplet sizes of different Pickering emulsions (A); size distributions of Pickering emulsions stabilized by individual ZCPs and CNCs as well as the complex interface with ZCPs as an inner layer (B); size distributions of Pickering emulsions stabilized by the complex interface with CNCs as an inner layer (C); zeta-potential of different Pickering emulsions (D) (Different superscript letters (a, b, c…) in the figure indicate significant differences ($p < 0.05$));

Fig. 3 Apparent viscosity of Pickering emulsions using ZCPs as an inner layer and CNCs as an outer layer (A); apparent viscosity of Pickering emulsions stabilized by CNCs as an inner layer and ZCPs as an outer layer (B); viscoelasticity of Pickering emulsions stabilized by ZCPs as an inner layer and CNCs as an outer layer (C); viscoelasticity of Pickering emulsions stabilized by CNCs as an inner layer and ZCPs as an outer layer (D);

Fig. 4 Physical stability of Pickering emulsions stabilized by ZCPs as an inner layer and CNCs as an outer layer (A); physical stability of Pickering emulsions stabilized by CNCs as an inner layer and ZCPs as an outer layer (B);

Fig. 5 Photo stability of β-carotene entrapped in Pickering emulsions (A); influence of thermal treatment on droplet size (B) and zeta-potential (C) of Pickering emulsions and chemical stability of β-carotene (D) (Different superscript letters (a, b, c…) in the figure indicate significant differences ($p < 0.05$));

Fig. 6 Effect of storage period on droplet size of Pickering emulsions (A), as well as retention rate of β-carotene entrapped in Pickering emulsions (B);

Fig. 7 The confocal images of different Pickering emulsions with the lipid droplets in green surrounded by a layer of ZCPs in red (Different superscript letters (a, b, c…) in

the figure indicate significant differences ($p < 0.05$));

Fig. 8 Impact of different pH values on the droplet size and zeta-potential of Pickering emulsions co-stabilized by ZCPs and CNCs (Different superscript letters (a, b, c…) in the figure indicate significant differences ($p < 0.05$));

Fig. 9 Influence of different ionic strengths on the droplet size and zeta-potential of Pickering emulsions co-stabilized by ZCPs and CNCs (Different superscript letters (a, b, c…) in the figure indicate significant differences ($p < 0.05$));

Fig. 10 Cryo-SEM microstructures of different Pickering emulsions;

Fig. 11 Digestion time dependence of FFA release (%) from different Pickering emulsions (A); bioaccessibility of β-carotene entrapped in different Pickering emulsions (B) (Different superscript letters (a, b, c…) in the figure indicate significant differences ($p < 0.05$)).

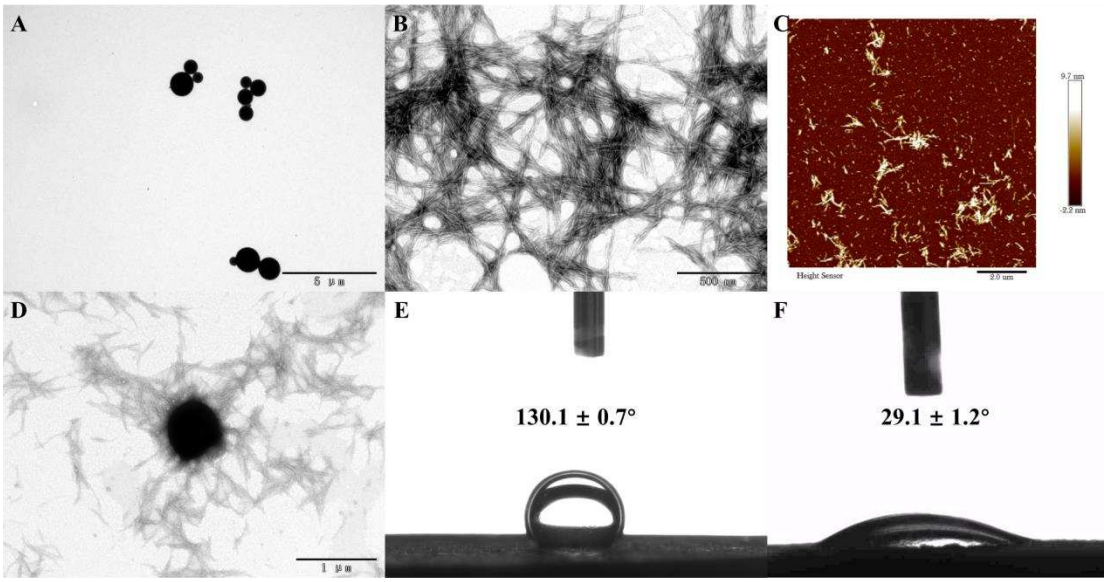

Fig. 1

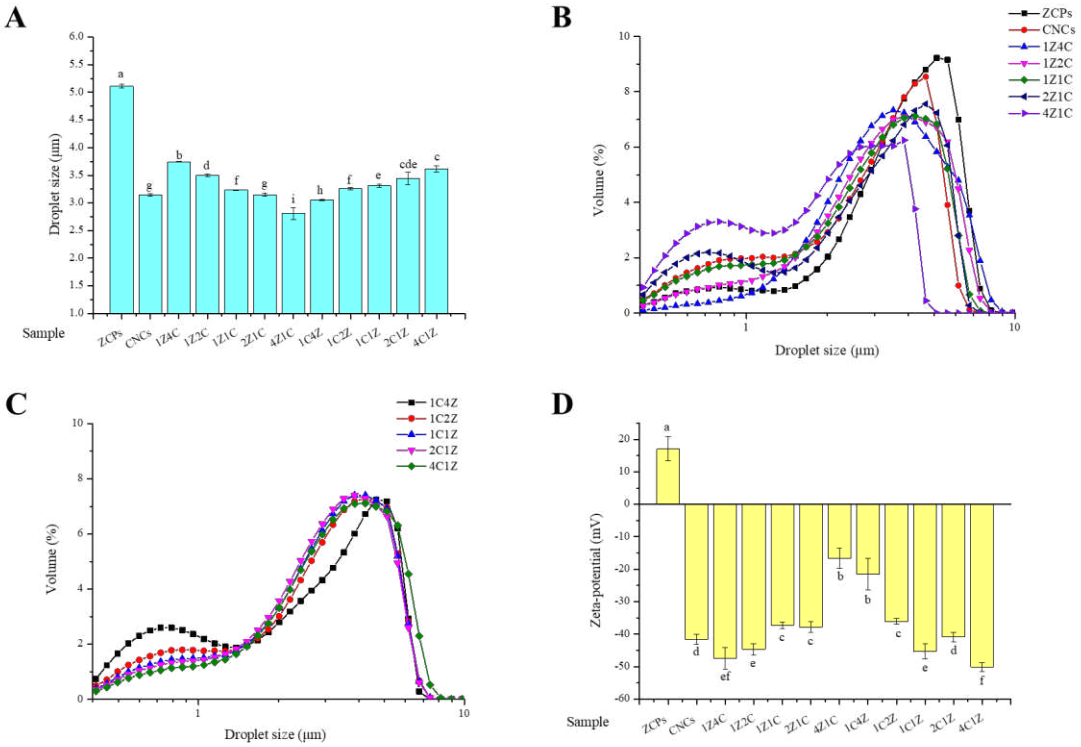
A
Droplet size (μm)
Sample
ZCPs
CNCs
1Z4C
1Z2C
1Z1C
2Z1C
4Z1C
1C4Z
1C2Z
1C1Z
2C1Z
4C1Z
B
Volume (%)
Droplet size (μm)
C
Volume (%)
Droplet size (μm)
D
Zeta-potential (mV)
Sample

Fig. 2

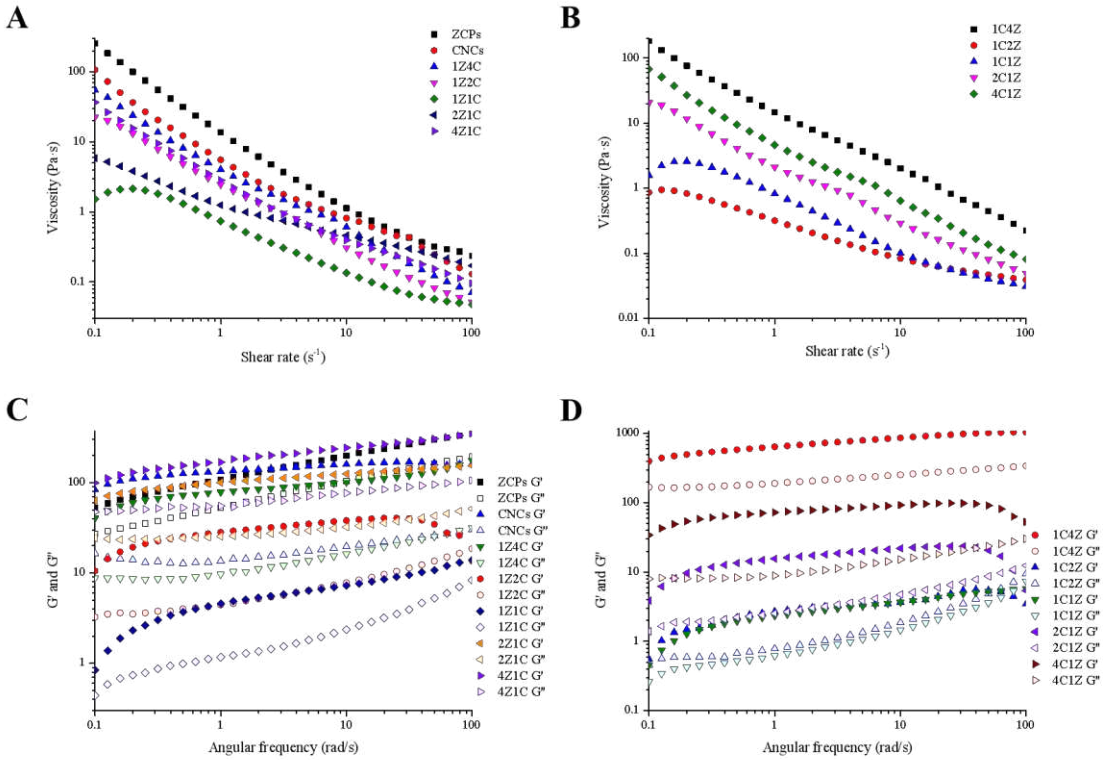
A
Viscosity (Pa·s)
Shear rate (s-1)
ZCPs
CNCs
1Z4C
1Z2C
1Z1C
2Z1C
4Z1C
B
Viscosity (Pa·s)
Shear rate (s-1)
1C4Z
1C2Z
1C1Z
2C1Z
4C1Z
C
G' and G"
Angular frequency (rad/s)
ZCPs G'
ZCPs G"
CNCs G'
CNCs G"
1Z4C G'
1Z4C G"
1Z2C G'
1Z2C G"
1Z1C G'
1Z1C G"
2Z1C G'
2Z1C G"
4Z1C G'
4Z1C G"
D
G' and G"
Angular frequency (rad/s)
1C4Z G'
1C4Z G"
1C2Z G'
1C2Z G"
1C1Z G'
1C1Z G"
2C1Z G'
2C1Z G"
4C1Z G'
4C1Z G"

Fig. 3

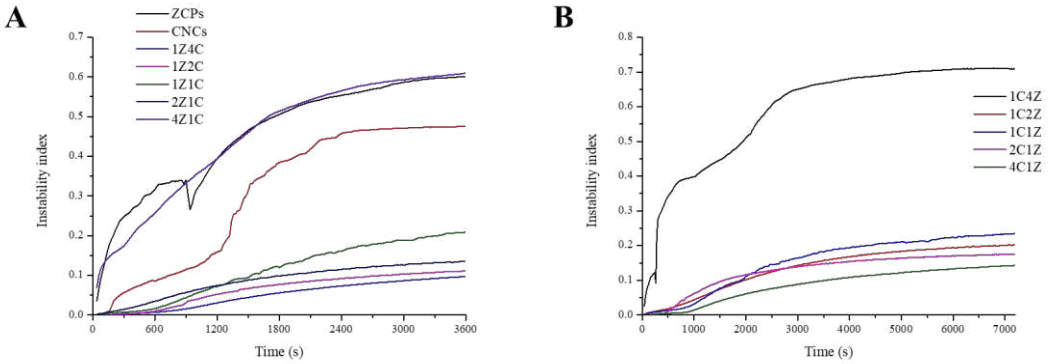
A
ZCPs
CNCs
1Z4C
1Z2C
1Z1C
2Z1C
4Z1C
Instability index
Time (s)
B
1C4Z
1C2Z
1C1Z
2C1Z
4C1Z
Instability index
Time (s)

Fig. 4

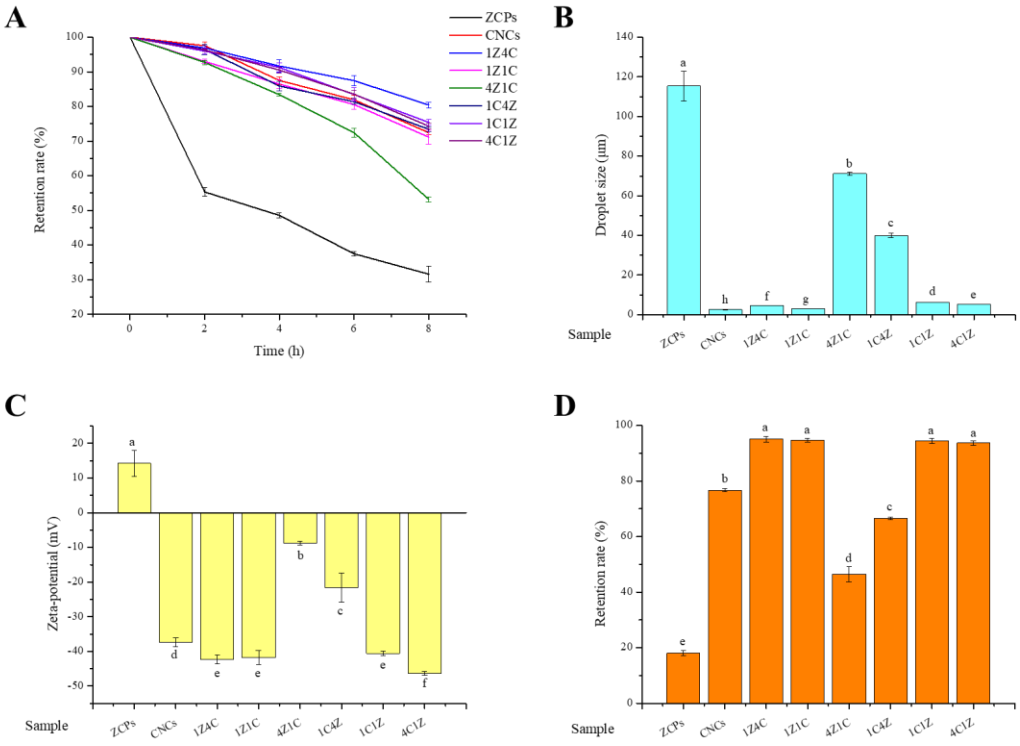
A
ZCPs
CNCs
1Z4C
1Z1C
4Z1C
1C4Z
1C1Z
4C1Z
Retention rate (%)
Time (h)
B
Droplet size (μm)
Sample
C
Zeta-potential (mV)
Sample
D
Retention rate (%)
Sample

Fig. 5

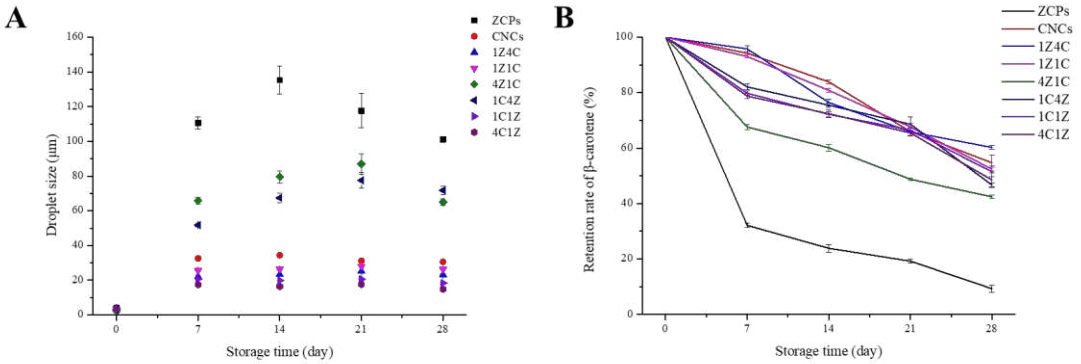
A
Droplet size (μm)
Storage time (day)
ZCPs
CNCs
1Z4C
1Z1C
4Z1C
1C4Z
1C1Z
4C1Z
B
Retention rate of β-carotene (%)
Storage time (day)
ZCPs
CNCs
1Z4C
1Z1C
4Z1C
1C4Z
1C1Z
4C1Z

Fig. 6

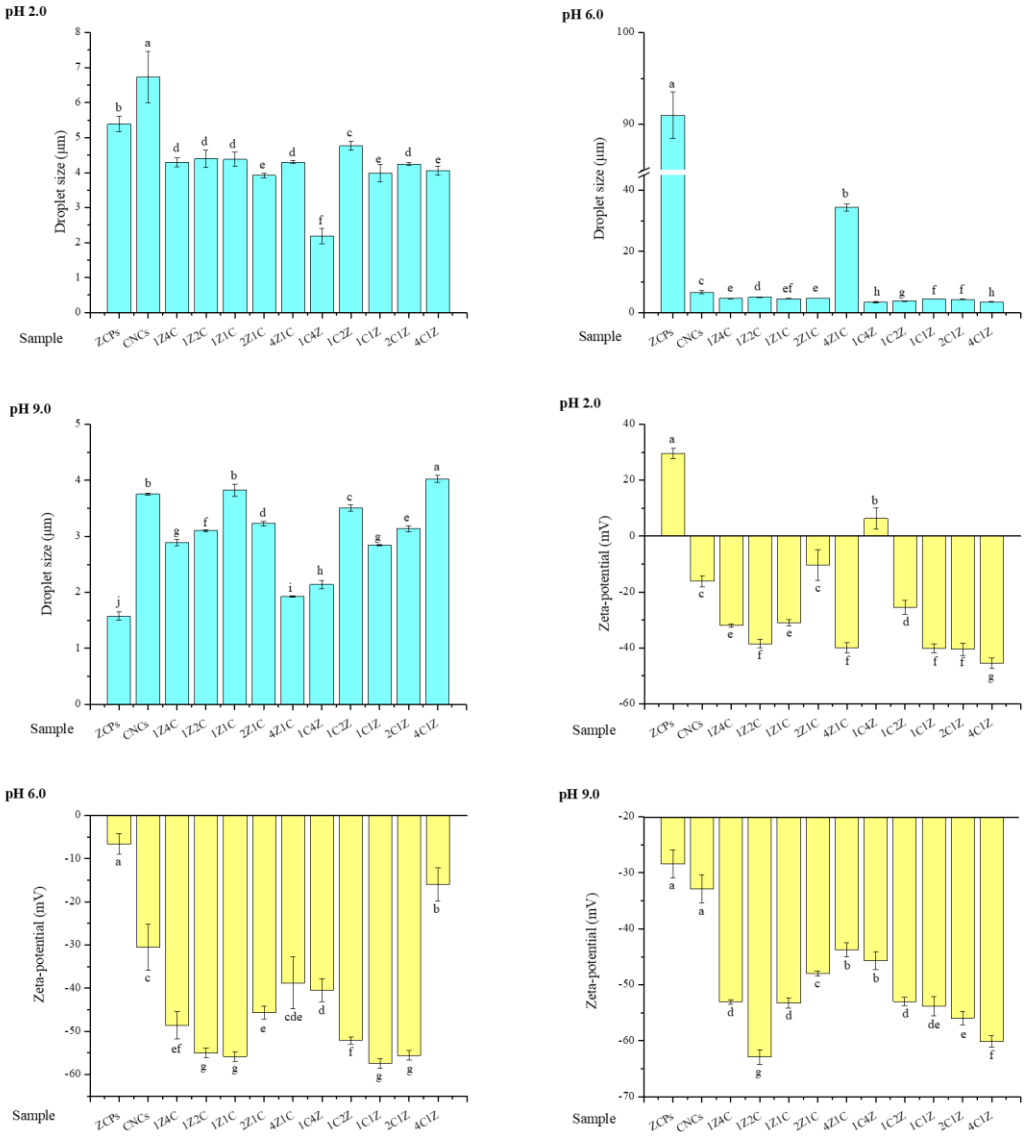
pH 2.0
Droplet size (μm)
Sample
ZCPs
CNCs
1ZAC
1Z2C
1Z1C
2Z1C
4Z1C
1CAL
1C2L
1C1L
2C1L
4C1L
pH 6.0
Droplet size (μm)
Sample
pH 9.0
Droplet size (μm)
Sample
pH 2.0
Zeta-potential (mV)
Sample
pH 6.0
Zeta-potential (mV)
Sample
pH 9.0
Zeta-potential (mV)
Sample

Fig. 7

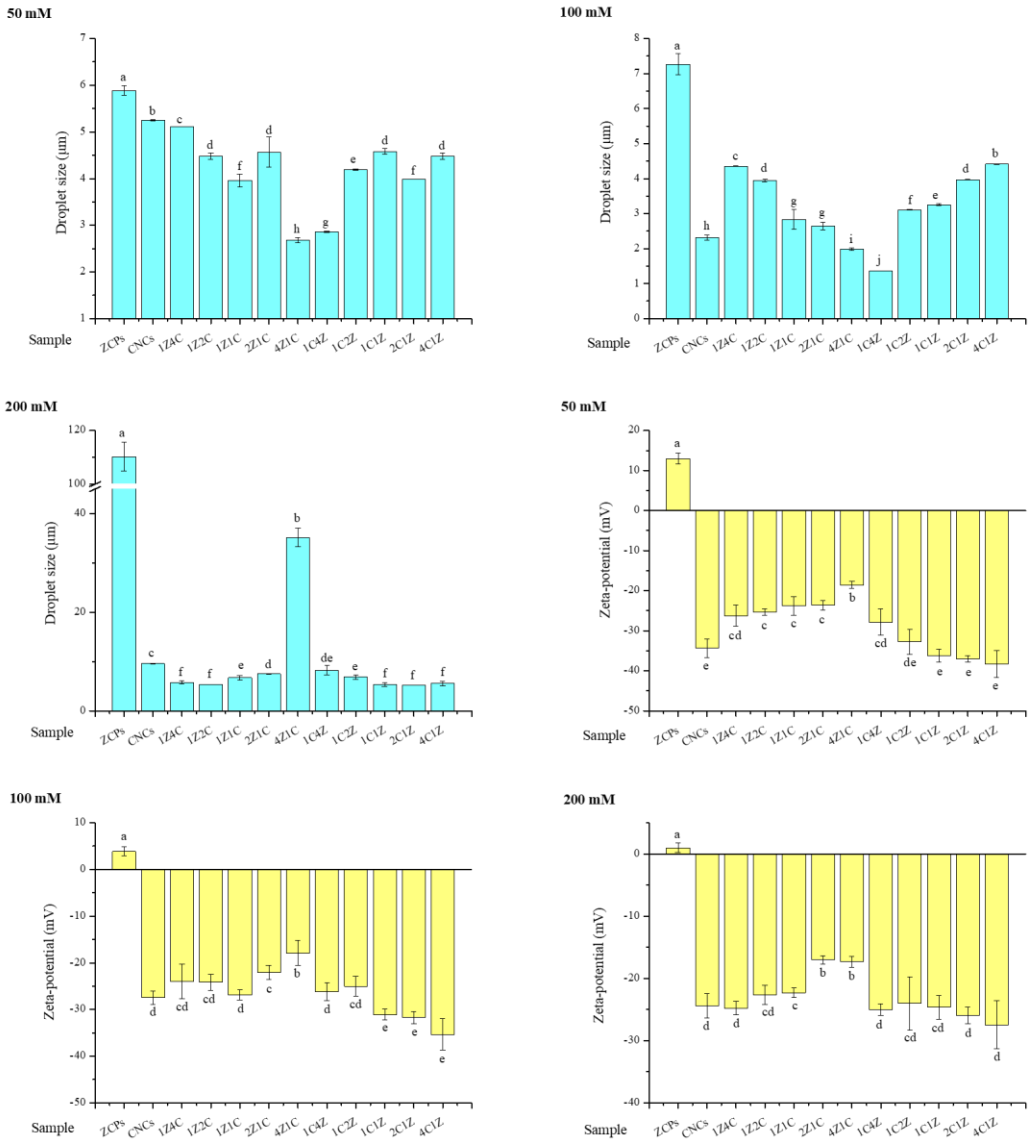
50 mM
100 mM
200 mM
50 mM
100 mM
200 mM
Droplet size (μm)
Zeta-potential (mV)
Sample
ZCPs
CNCs
1ZAC
1Z2C
1Z1C
2Z1C
4Z1C
1C4Z
1C2Z
1C1Z
2C1Z
4C1Z

Fig. 8

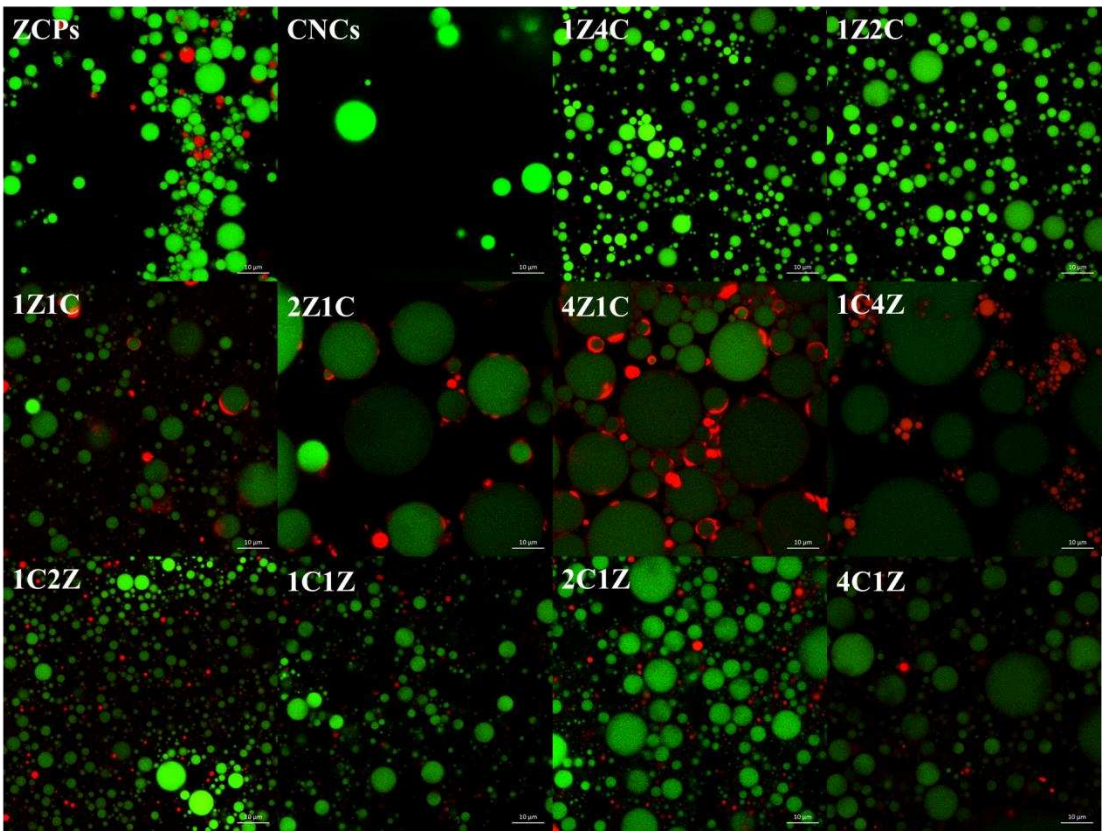

Fig. 9

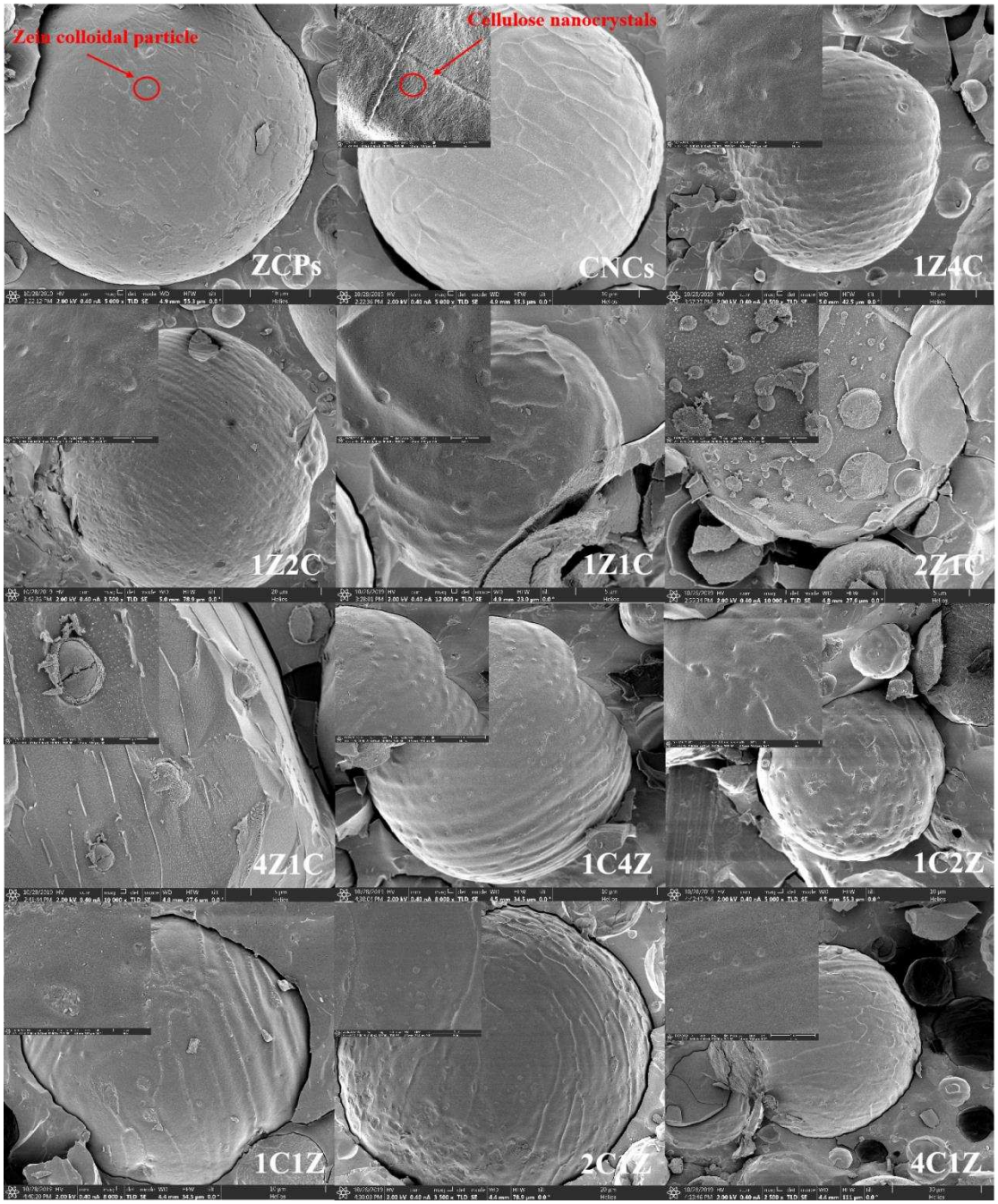
Zein colloidal particle
Cellulose nanocrystals
ZCPs
CNCs
1Z4C
1Z2C
1Z1C
2Z1C
4Z1C
1C4Z
1C2Z
1C1Z
2C1Z
4C1Z

Fig. 10

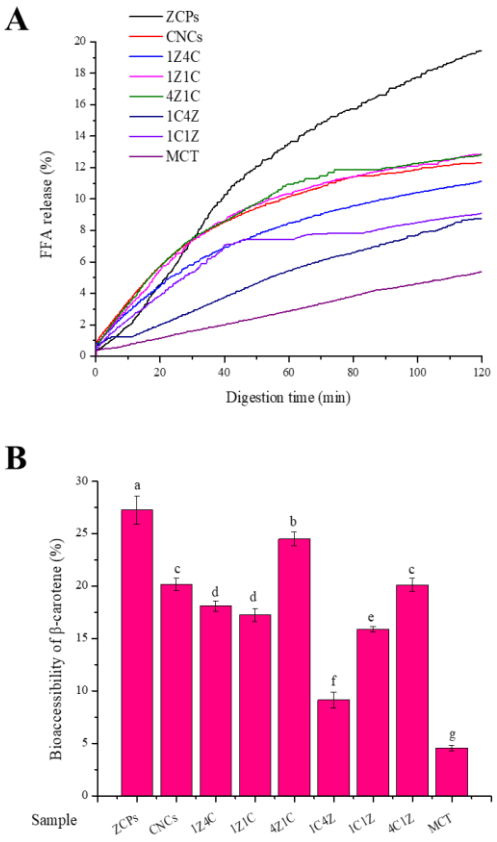
A
ZCPs
CNCs
1Z4C
1Z1C
4Z1C
1C4Z
1C1Z
MCT
FFA release (%)
Digestion time (min)
B
Bioaccessibility of β-carotene (%)
a
b
c
d
d
e
f
c
g
Sample
ZCPs
CNCs
1Z4C
1Z1C
4Z1C
1C4Z
1C1Z
4C1Z
MCT

Fig. 11